의학석사 학위논문

Microdosimetric simulation & its effect on cell cycle based on intratumoral radioisotope microdistribution in 3D tumor spheroids

3 차원 종양 스페로이드에서 방사성동위원소 미세분포에 따른 미세선량 시뮬레이션과 세포주기 영향

2023 년 02 월

서울대학교 대학원
의과학과 의과학전공
이 준 현

Master's Thesis of Science in Medicine

3 차원 종양 스페로이드에서 방사성동위원소 미세분포에 따른 미세선량 시뮬레이션과 세포주기 영향

Microdosimetric simulation & its effect on cell cycle based on intratumoral radioisotope microdistribution in 3D tumor spheroids

February 2023

The Department of Biomedical Science,
Seoul National University
College of Medicine
Junhyeon Lee

3차원 종양 스페로이드에서 방사성동위원소 미세분포에 따른 미세선량 시뮬레이션과 세포주기 영향

지도 교수 강 건 욱

이 논문을 의학석사 학위논문으로 제출함
2022년 10월

서울대학교 대학원
의과학과 의과학전공
이 준 현

이준현의 의학석사 학위논문을 인준함
2022년 12월

위 원 장 천 기 정 (인)

부위원장 강 건 욱 (인)

위 원 팽 진 철 (인)

Microdosimetric simulation & its effect on cell cycle based on intratumoral radioisotope microdistribution in 3D tumor spheroids

by
Junhyeon Lee

A thesis submitted to the Department of Biomedical Science in partial fulfillment of the requirements for the Degree of Master of Science in Medicine at Seoul National University College of Medicine

December 2022

Approved by Thesis Committee:

Professor Gi Jeong Cheon Chairman

Professor Keon Wook Kang Vice chairman

Professor Paeng, Jin Chul

학위논문 원문제공 서비스에 대한 동의서

본인의 학위논문에 대하여 서울대학교가 아래와 같이 학위논문 제공하는 것에 동의합니다.

1. 동의사항

① 본인의 논문을 보존이나 인터넷 등을 통한 온라인 서비스 목적으로 복제할 경우 저작물의 내용을 변경하지 않는 범위 내에서의 복제를 허용합니다.

② 본인의 논문을 디지털화하여 인터넷 등 정보통신망을 통한 논문의 일부 또는 전부의 복제.배포 및 전송 시 무료로 제공하는 것에 동의합니다.

2. 개인(저작자)의 의무

본 논문의 저작권을 타인에게 양도하거나 또는 출판을 허락하는 등 동의 내용을 변경하고자 할 때는 소속대학(원)에 공개의 유보 또는 해지를 즉시 통보하겠습니다.

3. 서울대학교의 의무

① 서울대학교는 본 논문을 외부에 제공할 경우 저작권 보호장치(DRM)를 사용하여야 합니다.

② 서울대학교는 본 논문에 대한 공개의 유보나 해지 신청 시 즉시 처리해야 합니다.

논문 제목: Microdosimetric simulation & its effect on cell cycle based on intratumoral radioisotope microdistribution in 3D tumor spheroids

학위구분: **석사 ▣ · 박사 □**
학 과: 의과학과
학 번: 2020-28141
연 락 처: 010-5380-5661
저 작 자: 이 준 현 (인)

제 출 일: 2023 년 02 월 06 일

서울대학교총장 귀하

ABSTRACT

Introduction: In radiopharmaceuticals, calculating the absorbed dose is essential because the absorbed dose determines the cellular response and therapeutic effects of the tumor. However, basic research on absorbed dose within the tumor is still insufficient. The therapeutic effect of radiopharmaceuticals can be predicted by measuring the distribution of radiopharmaceuticals within 3D tumor spheroids and calculating changes in absorbed dose for various parameters.

Methods: For therapeutic radioiodine ^{131}I delivery, sodium iodide symporter (NIS) was expressed in cells constituting 3D tumor spheroids. The activity distribution was measured by dissociating 3D tumor spheroids. MIRDcell was used to calculate the absorbed dose and cell survival response of 3D tumor spheroids. Cell cycle analysis of 3D tumor spheroids was analyzed by imaging a fluorescent ubiquitination-based cell cycle indicator (Fucci) expressed in cells.

Results: The activity of ^{131}I versus distance from the center of a 3D tumor spheroid was fitted to a lognormal curve. Depending on the activity distribution, the absorbed dose at the center of the

3D tumor spheroid differs more than five times. At a constant max mean activity per cell, ^{131}I with low ionization energy and high penetration range damages more cells than ^{211}At with high ionization energy and low penetration range. Substitute activity residence time with the 'time-integrated activity coefficient (1.44 × physical half-life of ^{131}I)' yields a cell survival fraction < 0.1%, whereas substituting radioactive residence time with 'cellular residence time (1.44 × cellular half-life of ^{131}I)' yields a cell survival fraction higher than 10%. Cell survival fraction decreased as the number of cells labeled with ^{131}I increased, but labeled cells did not die significantly more than unlabeled cells. Although the activity is almost distributed outside the 3D tumor spheroid, the absorbed dose range covers the entire 3D tumor spheroid. As a result of cell cycle analysis, cell cycle arrest was observed in the absorbed dose range of 3D tumor spheroids. **Conclusions:** This study demonstrated the potential of 3D tumor spheroids as a preclinical tumor model for basic research into radiopharmaceuticals. MIRDcell has been evaluated as a tool for microdosimetry and prediction of cell survival response. Applying MIRDcell simulation of 3D tumor spheroids to radiopharmaceutical research requires understanding preclinical

and clinical differences. The distribution of radiopharmaceuticals in tissues, the residence time of radiopharmaceuticals within cells, and the cellular uptake of radiopharmaceuticals differ between preclinical and clinical studies. Estimating these biological parameters solely through computations may be inappropriate. Because biological parameters significantly impact microdosimetry, parameter determination experiments should precede dosimetry simulations.

Keywords: microdosimetric simulation, 3D tumor spheroid, MIRDcell, radioiodine ^{131}I, activity per cell, absorbed dose to cells, activity distribution, cell survival response, fluorescent ubiquitination-based cell cycle indicator (Fucci),
Student number: 2020-28141

CONTENTS

LIST OF TABLES

LIST OF FIGURES

LIST OF ABBREVIATION

3D, Three dimensional

^{131}I, Iodine 131

BSA, Bovine serum albumin

FBS, Fetal bovine serum

Fucci, Fluorescent ubiquitination-based cell cycle indicator

HBSS, Hank's balanced salt solution

LQ model, Linear-quadratic model

MIRD, Medical internal radiation dose

NIS, Sodium iodide symporter

PE, Plate efficiency

SDS, Sodium dodecyl sulfate

SF, Survival fraction

INTRODUCTION

The key to radiation therapy is to deliver ionizing radiation only to tumor cells while minimizing damage to normal tissue. There are two methods of delivering ionizing radiation to tumors: external-beam radiation therapy and radiopharmaceutical therapy. External-beam radiation therapy irradiates the tumor with photons, electrons, protons, or other particles by adjusting the absorbed dose and transmission range to a certain level. Although beam radiation therapy accurately predicts the absorbed dose to the tumor and minimizes damage to normal tissue, it is difficult to use for micrometastases (1, 2). Radiopharmaceutical therapy irradiates the tumor with alpha, beta, or gamma rays by binding radiopharmaceutical to chemical or biological targets on tumor cells. Radiopharmaceutical therapy is more beneficial for sterilizing disseminated tumor cells, circulating tumor cells, and micrometastases than external irradiation therapy. However, the absorbed dose to the tumor varies depending on the type of radiation, the radiation's excess energy, and the radiopharmaceutical distribution within tumors (3, 4). Calculating of the absorbed dose is essential because the

absorbed dose determines the cellular response and therapeutic effect on cancer. However, basic research on the treatment effect on absorbed dose within the tumor is still insufficient (1–3). In particular, radiobiological studies on models that similarly reflect tumors in preclinical conditions are required. Therefore, various tumor models have been proposed to study radiopharmaceuticals' physically absorbed dose and biological response to cells in preclinical studies.

The most representative *in vitro* method among various tumor model generation methods is a 3D cell culture that reflects the 3D environment in which tumors grow (5–8). 3D tumor spheroids formed by 3D cell culture have a similar morphology to *in vivo* tumors even though they are included *in vitro*. Significantly, in 2D cells, all cells are continuously exposed to the culture medium, whereas in 3D tumor spheroids, the degree of exposure to the culture medium depends on their physical structure (5, 6). In preclinical studies, the degree of exposure of the tumor model to the culture medium is significant because the therapeutic effect must be evaluated by exposing radiopharmaceuticals mixed in the cell culture medium (9, 10). The therapeutic effect of radiopharmaceuticals in microtumors

can be predicted by measuring the distribution of radiopharmaceuticals within 3D tumor spheroids and calculating the absorbed dose to cells.

Medical Internal Radiation Dose (MIRD) formalism is a method of calculating absorbed dose by combining the biodistribution of radiopharmaceuticals and the physical properties of radionuclides (11, 12). The MIRD committee released MIRDcell, software tools for bioeffect and dosimetric modeling of radiopharmaceuticals (2, 13). Using MIRDcell, absorbed dose and cell survival responses can be modeled in single cells and cell populations.

This study aims to calculate the absorbed dose to cells depending on the biological parameters of radiopharmaceutical therapy in 3D tumor spheroids and to analyze the effects on treatment efficacy and cell cycle. For therapeutic radioiodine ^{131}I delivery, sodium iodide symporter (NIS) was expressed in cells constituting 3D tumor spheroids, and ^{131}I distribution was measured by dissociating 3D tumor spheroids. MIRDcell was used to calculate the radiation absorbed dose and cell survival response of 3D tumor spheroids. Cell cycle analysis of 3D tumor

spheroids was analyzed by imaging a Fluorescent ubiquitination-based cell cycle indicator (Fucci) expressed in cells(24-26).

MATERIAL AND METHODS

Establishment of hNIS-expressing cell lines

HeLa cells and HeLa-Fucci(CA)2 cells were selected as target cells for NIS-expressing transduction. HeLa cells were obtained from Korea Cell Line Bank (Seoul, Korea). HeLa-Fucci(CA)2 cells were obtained from Riken BRC (Tsukuba, Japan) through the National Bioresource Project of MEXT, Japan. 293FT cells were selected as packaging cells for viral vectors and were purchased from Invitrogen (Carlsbad, CA, USA). HeLa cells and HeLa-Fucci(CA)2 cells were cultured in DMEM (WelGENE, Daegu, Korea) containing 10% heat-inactivated FBS (Thermo Scientific, Palm Springs, CA, USA) and 1% antibiotics (penicillin-streptomycin, Thermo Scientific) at 37°C in 5% CO2. 293FT cells were maintained in complete DMEM(WelGENE) with 2 mM L-Glutamine (Gibco, Grand Island, NY, USA), 1 mM Sodium pyruvate (Gibco), and 1% MEM NEAA (Gibco).

A codon-optimized human NIS (hNIS) retrovirus was constructed as in the previous study (14). Briefly, retroviruses were generated using a modification of the Retro-X universal packaging system (BD Biosciences Clontech, Palo Alto, CA, USA). 293FT packaging cells were transducted with 5 μg

pMSCV/hNIS vector, 5 μg pcDNA3-gag-pol vector, and 5 μg envelope vector, using Lipofectamine 2000 (Invitrogen). Supernatants were collected 72 hours after transduction and filtered through a 0.45 μm polyvinylidene difluoride (PVDF) filter (Sigma-Aldrich, St. Louis, MO, USA). Viral supernatants were titrated and stored at −80 °C.

One day before infection with retroviral vectors, cells were seeded in 6-well plates in serum-free medium at a density of 2×10^5 cells/well. Cells were infected by exposing the cell monolayer to retrovirus in the presence of 10 μg/mL polybrene (Sigma-Aldrich) for 12 hours. After 12 hours of incubation, retrovirus-infected cells were added to the complete medium and grown overnight. After 48 h incubation in the complete medium, positive cells (HeLa-hNIS, HeLa-Fucci/hNIS) were selected using 1.5 μg/mL puromycin (Sigma-Aldrich).

Expression of NIS was evaluated by western blot. Cells were lysed in Pierce IP Lysis Buffer (Thermo Scientific) with protease inhibitor cocktail (Roche Diagnostics, Basel, Switzerland) and then cleared by centrifugation (14,000 × g for 20 minutes at 4℃). Protein concentrations were determined using the Pierce BCA Protein Assay kit (Thermo Scientific). Total protein (30 μg)

mixed with 4X polyacrylamide gel electrophoresis sample buffer (Invitrogen) was separated through bis-Tris·HCl buffered 4%-12% gradient polyacrylamide gels (Invitrogen) and transferred to nitrocellulose membranes. Membranes were blocked with 5% skim milk in TBS-T (20 mM Tris, Sigma-Aldrich, 137 mM NaCl, Sigma-Aldrich, and 0.1% Tween 20, Sigma-Aldrich) for 1 hour at room temperature and then incubated with following primary antibody overnight at 4℃, anti-hNIS (Koma Biotech, Seoul, South Korea; diluted 1:1000) or β-actin (Sigma-Aldrich; diluted 1:5000). Antigen-antibody complexes were visualized with HRP-conjugated secondary antibody (Sigma-Aldrich; diluted 1:2000) and enhanced chemiluminescence detection reagent (Thermo Fisher Scientific). The signal intensity was then measured using a ChemiDoc imaging system (Bio-Rad, Hercules, CA, USA).

Technetium-99m pertechnetate ($[^{99m}Tc]NaTcO_4$) uptake was performed to evaluate the function of expressed NIS. Cells were seeded into T75 flasks one day earlier. Cells were trypsinized, washed with warm HBSS (10% HBSS, Gibco, 4.17 mM $NaHCO_3$, Sigma-Aldrich, 10.07 mM HEPES, Sigma-Aldrich, 5 mg/ml BSA, GenDepot, Katy, TX, USA), and incubated with 1 ml of warm

medium containing 37 kBq/ml of [^{99m}Tc]$NaTcO_4$ at 37°C for 30 minutes. Cells were washed twice with cold HBSS. Cells were harvested, and radioactivity was measured using a gamma counter (PerkinElmer, Waltham, MA, USA). After the measured cells were lysed in 1% SDS for 5 minutes, the radioactivity was normalized to the total amount of protein at the analysis time using the Pierce BCA Protein Assay kit.

Estimation of biological equivalent absorbed dose

Iodine-131 sodium iodide ([^{131}I]NaI) uptake was tested in 2D cells to calculate [^{131}I]NaI uptake times and radioactive concentrations for 3D tumor spheroid experiments. Cells were seeded into T75 flasks one day earlier. Cells were trypsinized and washed with warm HBSS (10% HBSS, Gibco, 4.17 mM $NaHCO_3$, Sigma-Aldrich, 10.07 mM HEPES, Sigma-Aldrich, 5 mg/ml BSA, GenDepot, Katy, TX, USA, 90% distilled water). The trypsinized cells were incubated with 1 ml of warm medium containing 1.48-5.92 MBq/ml of [^{131}I]NaI and 10 μM non-radioactive NaI at 37°C for 30 minutes. Cells were washed twice with cold HBSS. The radioactivity of harvested cells was counted

using a gamma counter (PerkinElmer). Cells were lysed with 1% SDS to normalize the amount of protein in cells.

A clonogenic survival assay was performed to evaluate the treatment efficacy of [^{131}I]NaI uptake and to calculate the biological equivalent absorbed dose of external radiation. Cells were trypsinized and washed with warm HBSS (10% HBSS, Gibco, 4.17 mM $NaHCO_3$, Sigma-Aldrich, 10.07 mM HEPES, Sigma-Aldrich, 5 mg/ml BSA, GenDepot, Katy, TX, USA, 90% distilled water). The trypsinized cells were incubated with 1 ml warm medium containing 1.48-5.92 MBq/ml of [^{131}I]NaI and 10 μM non-radioactive NaI at 37°C for 30 minutes. Cells were washed twice with cold HBSS and seeded in T25 flasks. To compare these results with external irradiation, cells were seeded in T25 flasks and irradiated with 1-10 Gy of ^{137}Cs γ-ray irradiator (CIS IBL 473C). After 8 days, the cell colonies were stained with a crystal violet solution (2 mg/ml crystal violet, Sigma-Aldrich, 10% of 40% formaldehyde, Sigma-Aldrich, 20% ethanol, Sigma-Aldrich, 70% distilled water). The mean and standard deviation of plate efficiency (PE) and survival fraction (SF) were calculated. The calculated SF was fitted to a linear-quadratic model (Equation 1).

Equation 1. $$SF = e^{-(\alpha D+\beta D^2)}$$

Radioactivity distribution of [^{131}I]NaI in 3D tumor spheroids

3D tumor spheroids were generated using round bottom-96 well plates (Corning, NY, USA). 1×10^3 - 2×10^4 cells were plated in each well and incubated for about 4 days.

The radioactivity of [^{131}I]NaI uptake in 3D tumor spheroids was counted. 3D tumor spheroids were treated with 100 μl of 4.44 MBq/ml [^{131}I]NaI and incubated for 30 minutes. [^{131}I]NaI was removed and washed twice with ice-cold HBSS (10% HBSS, Gibco, 4.17 mM $NaHCO_3$, Sigma-Aldrich, 10.07 mM HEPES, Sigma-Aldrich, 5 mg/ml BSA, GenDepot, Katy, TX, USA, 90% distilled water). 3D tumor spheroids were harvested and the radioactivity of 3D tumor spheroids was counted using a gamma counter (PerkinElmer). 3D tumor spheroids were dissolved with cell dissociation reagent (Accutase, Gibco) for normalization to cell number.

To determine the release time of [^{131}I]NaI in 3D tumor spheroids, the radioactivity released was counted after washing the 3D tumor spheroids. 3D tumor spheroids were treated with 100 μl of 4.44 MBq/ml [^{131}I]NaI and incubated for 30 minutes.

[^{131}I]NaI was removed and washed twice with 100 μl ice-cold HBSS. 100ul of cold HBSS was added and incubated for a few minutes. Then the existing HBSS was obtained and replaced with fresh HBSS. This was repeated at intervals of 5, 10, 30, 50, 60, 80, 100, 120, 180, 300, and 1080 minutes. Radioactivity remaining in the obtained HBSS and 3D tumor spheroids was measured. The radioactivity remaining in the 3D tumor spheroid was calculated by setting the sum of all radioactivity and residual radioactivity in the 3D tumor spheroid to 100%. The % cell radioactivity was fitted to an exponential decay equation (Equation 2) to calculate the cellular residence time (1.44 × cellular half-life of ^{131}I).

Equation 2. $$A = (A_0 - NS)e^{-\frac{\ln 2 \cdot t}{T_{1/2}}} + NS$$

*A_0= radioactivity (%)

*t= time (minutes)

*$T_{1/2}$= cellular half-life

*NS=nonspecific binding at $t \to \infty$

To analyze the radioactivity distribution of [^{131}I]NaI in the 3D tumor spheroid, the 3D tumor spheroid was dissolved and the radioactivity of [^{131}I]NaI in the 3D tumor spheroid was counted (Figure 1). 3D tumor spheroids were treated with 100 μl of 4.44 MBq/ml [^{131}I]NaI and incubated for 30 minutes. [^{131}I]NaI was removed and washed twice with HBSS(10% HBSS, Gibco, 4.17 mM $NaHCO_3$, Sigma-Aldrich, 10.07 mM HEPES, Sigma-Aldrich, 5 mg/ml BSA, GenDepot, Katy, TX, USA, 90% distilled water). 20 μl of cell dissociation reagent (Accutase, Gibco) was added to the 3D tumor spheroids and gently shaken twice to sequentially dissolve. Obtain cells and add 20 μl of fresh cell dissociation reagent. The mean absorbed dose per cell obtained by repeating this process was measured.

It was assumed that single cells and 3D tumor spheroids were spherical, that the diameters of single cells were constant, and that the diameters of single cells were constant. It was assumed that single cells were randomly populated into the 3D tumor spheroid. The activity distribution of the 3D tumor spheroid was calculated using the spherical volume formula. The activity distribution of the 3D tumor spheroids was calculated using the formula for the volume of the sphere (volume of the sphere =

$4/3\ \pi r^3$, the density of cell packing = 63.5%). 3D tumor spheroids were dissolved with cell dissociation reagent (Accutase, Gibco) for normalization to cell number. Results were fitted to lognormal (Equation 3), cubic polynomial (Equation 4), Quadratic polynomial (Equation 5), and linear (Equation 6).

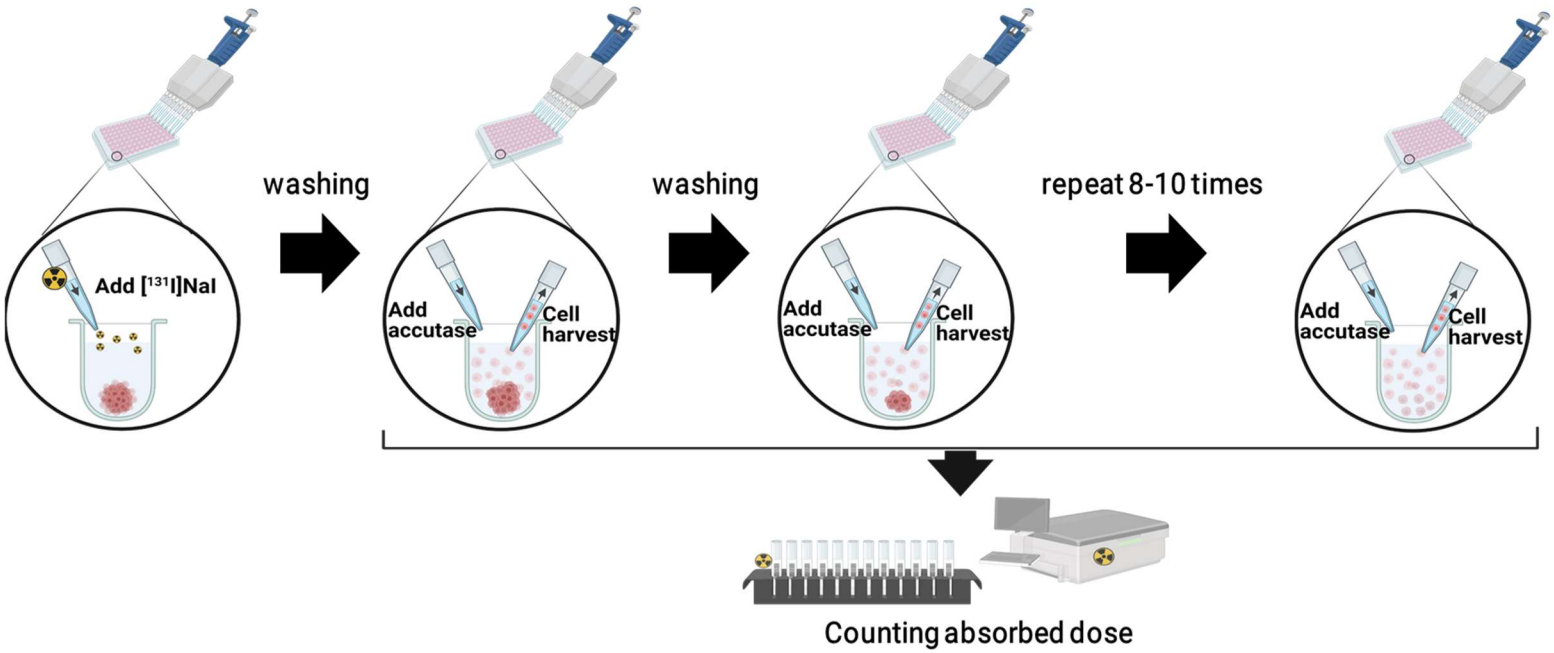

Figure 1. Schematic measurement of radioactivity distribution in a 3D tumor spheroid

Equation 3. $$A(r) = y_0 + \left(\frac{a}{r}\right) exp\left[\left(\frac{1}{2}\right) \cdot \left(\frac{ln\left(\frac{r}{x_0}\right)}{b}\right)^2\right]$$

*x_0, y_0, a, b = parameters set by experiment

Equation 4. $$A(r) = a_0 + a_1 r + a_2 r^2 + a_3 r^3$$

*a_n = polynomial coefficients set by experiment

Equation 5. $$A(r) = a_0 + a_1 r + a_2 r^2$$

*a_n = polynomial coefficients set by experiment

Equation 6. $$A(r) = f(R - r) + r$$

$$*f = \frac{\text{activity per cell at center}}{\text{activity per cell at edge}}$$

A = mean cellular radioactivity by radial distance from center of 3D tumor spheroids

r = radial distance of center of cell from center of 3D tumor spheroids

R = radius of 3D tumor spheroids

MIRDcell simulation of absorbed dose and cell survival response to cells in 3D tumor spheroids

MIRDcell V3.12 was used to model radionuclide-labeled 3D tumor spheroids and to simulate absorbed dose and cell survival responses per single cell (11, 12, https://mirdsoft.org). Simulations of absorbed dose and cell survival responses in the 3D tumor spheroid model were performed separately using the following parameters as independent variables:

1. Distribution of radioactivity
2. Types of radionuclides
3. Time-integrated activity coefficient (residence time)
4. Proportion of radionuclide (^{131}I) labeled cells

1. Distribution of radioactivity

The distribution of radioactivity in the 3D tumor model was established as a lognormal (Equation 2), cubic polynomial (Equation 3), quadratic polynomial (Equation 4), and linear (Equation 5) model fitted to the experimental values. Table 2 summarizes the equations and parameters. The lognormal distribution was selected as the baseline model for other experiments.

2. Types of radionuclides

The β average energy spectrum of ^{131}I used in the *in vitro* experiment was selected as a control radionuclide. The average energy spectrum of α-ray emitter ^{211}At+daughters and the average energy spectrum of auger electron and γ-ray emitter ^{123}I were set as experimental radionuclides. Although each of nuclides emit different types of radiation, all are mediated by NIS.

3. Time-integrated activity coefficient (residence time)

The time-integrated activity coefficient was calculated as $1.44T_{1/2}$, the residence time formula for exponential decay. The time-integrated activity coefficient for the physical half-life of ^{131}I is 277.77 hours. Based on the [^{131}I]NaI efflux experiments in 3D tumor spheroid, the residence time of ^{131}I in cells is 3.68 hours.

4. Proportion of radionuclide (^{131}I) labeled cells

The upper limit of the percentage of labeled cells (ratio of unlabeled cells to cells labeled with ^{131}I) was set at 100%, and the lower limit was set at 5%.

For β average energy spectra, MIRDcell software's input data was used. The cells were modeled in MIRDcell two concentric spheres representing the cell nucleus and the cell. All cells in the 3D tumor spheroid were assembled from identically sized HeLa cells with a cell radius of 8 μm and a nuclear radius of 2 μm (28). The spacing between centers was set at 16 μm. The 3D tumor spheroid was a sphere with a radius of 750 μm. The cell count in 3D tumor spheroid of close-packed cubic geometry was 431545.

All radioactivity was set to be distributed in the cytoplasm (source region = cytoplasm), reflecting that NIS transports iodine from outside the cell membrane to the cytosol. Because ionizing radiation emitted from radionuclides kills cells by causing DNA damage in the cell nucleus, the target region was set to the cell nucleus. The effect of photon radiation was neglected.

MIRDcell V3.12 has two methods for setting radiobiological parameters to simulate the cell survival response. One is a simple radiobiological parameter that sets the same linear-quadratic model parameter value regardless of the type of radiation and 'source region → target region' within the cell. The other is a complex radiobiological parameter that can distinguish linear-

quadratic model parameter values depending on the type of radiation and intracellular "source region→target region." Since the clonogenic assay for absorbed dose was experimented only with gamma rays, simple radiobiological parameters were selected. The linear-quadratic model parameter values were summarized in Table 1. The 'max mean activity per cell (all cells)' was measured as [^{131}I]NaI uptake in 3D tumor spheroids. After measuring the CPM value of the 3D tumor spheroid, the CPM value was converted into DPM and Bq using the counting efficiency of the γ-counter. The measured activity was divided by the number of dissociated 3D tumor spheroid cells.

Induced cell cycle arrest with [^{131}I]NaI uptake in 3D tumor spheroids

Cell cycle analysis was performed using the fluorescent ubiquitination-based cell cycle indicator, Fucci(CA)2 (Riken) (24-26).

Fucci(CA)2 responds to cell cycle changes by emitting red fluorescence in the G1 phase, green in the S phase, and yellow fluorescence in G2 and M phases (Figure 2)(24). Hydroxyurea (HU, Sigma-Aldrich), which arrests the cell cycle in the S phase, was used to evaluate of Fucci-expressing cells. HeLa-Fucci(CA)2 cells and HeLa-Fucci(CA)2-hNIS cells were each plated at 2×10 4, 8-well chamber cover glass (Thermo Fisher). After 24 hours, the existing medium was replaced with a 200 μM HU (Sigma-Aldrich) diluted in medium without phenol red. The fluorescence distribution of Fucci in cells was imaged for 48 h at 24 h intervals using a confocal laser scanning microscope (Olympus).

After generating 3D tumor spheroids using HeLa-Fucci and HeLa-Fucci-hNIS cells, 100 ul of 4.44 MBq/ml [^{131}I]NaI mixed medium was added and incubated for 30 minutes. After washing twice with HBSS(10% HBSS, Gibco, 4.17 mM $NaHCO_3$, Sigma-

Aldrich, 10.07 mM HEPES, Sigma-Aldrich, 5 mg/ml BSA, GenDepot, Katy, TX, USA, 90% distilled water), phenol red-free medium(WelGENE) has been added. The fluorescence distribution of Fucci in 3D tumor spheroids was imaged for 24 h at 6 h intervals using a confocal laser scanning microscope (Olympus).

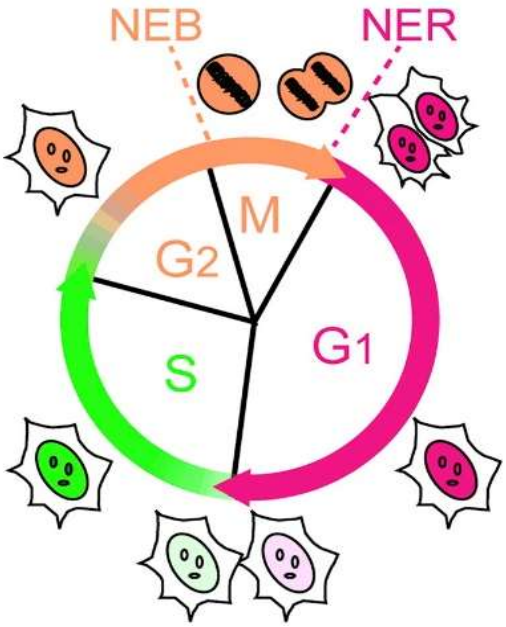

Figure 2. Schematic of fluorescence ubiquitination-based cell cycle indicator

Statistical analysis

All results were calculated as mean ± standard deviation (SD). Statistical significance was determined using an unpaired 2-sample parametric Student t-test. GraphPad Prism 9 software (GraphPad Software Inc., San Diego, CA, USA) was used for statistical analysis. $p < 0.05$ was considered statistically significant.

RESULTS

Establishment of hNIS-expressing cell line

The HeLa-hNIS cell line was constructed using the pMSCV-codon optimized human sodium iodide symporter (hNIS) vector. The hNIS protein appeared in both unglycosylated (72 kDa) and glycosylated (97-170 kDa) forms in hNIS-transformed cells (Figure 3A). Glycosylated hNIS protein was differentially expressed in proportion to the dose of retrovirus treated, and expression was not observed in non-transduced HeLa cells.

The function of hNIS was evaluated through [^{99m}Tc]$NaTcO_4$ uptake experiments (Figure 3B). Radioactivity uptake of [^{99m}Tc]$NaTcO_4$ is measured as counts per minute per mg of intracellular protein (CPM/mg). The CPM values measured in HeLa-hNIS cells were more than 100-fold higher than in HeLa cells. When $NaClO_4$ was used to block the uptake of NaI by hNIS, the CPM values decreased to a level similar to that of the HeLa cells.

(A)

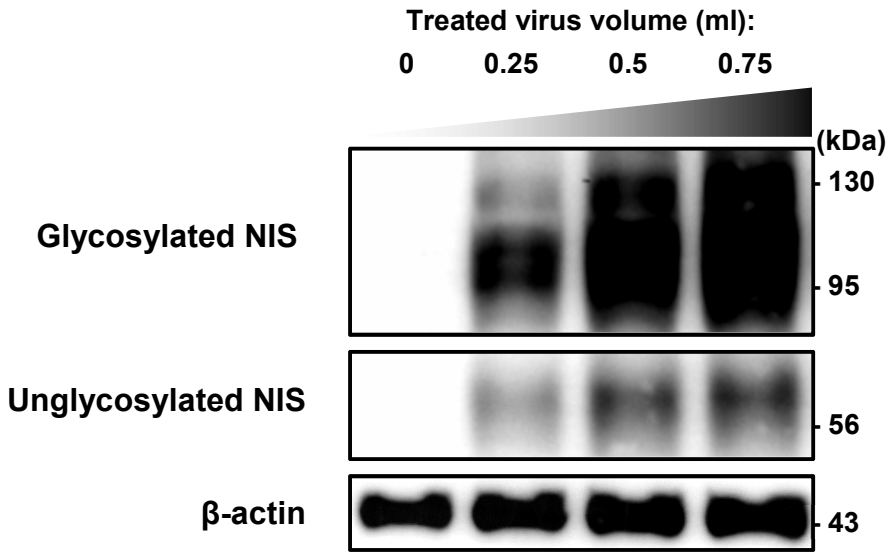

(B)

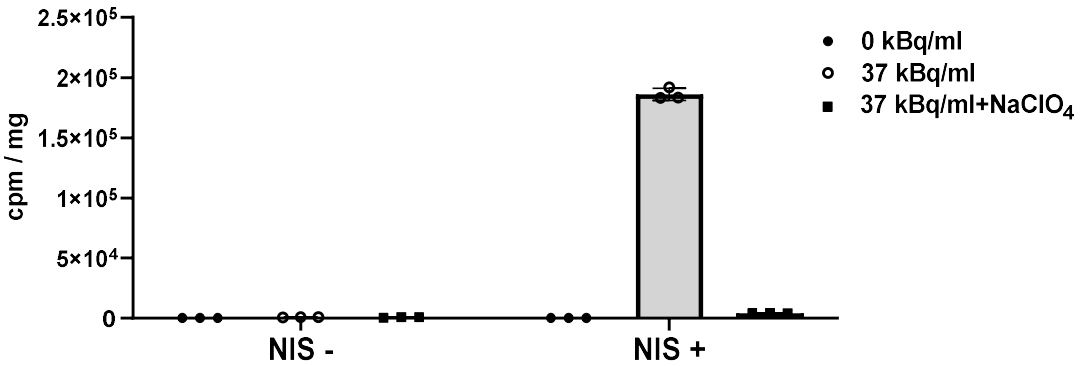

Figure 3. Establishment of hNIS-expressing cell line

(A) Western blot analysis of NIS protein in HeLa-hNIS cells.; (B) [^{99m}Tc]$NaTcO_4$ uptake assay in HeLa-hNIS cells. $NaClO_4$ was used as the blocking agent. Data represent mean ± SD (n = 3 per group;

Estimation of biological equivalent absorbed dose

To determine the uptake time and uptake activity of 3D tumor spheroid experiments and clonogenic assay, [^{131}I]NaI uptake assay in 2D cells was performed. (Figure 4A). HeLa-hNIS cells incubated with [^{131}I]NaI concentrations ranging from 1.48 MBq/ml to 5.92 MBq/ml were set as experimental groups. HeLa-hNIS cells incubated with non-radioactive NaI (0 MBq/ml) and HeLa cells incubated with 5.92 MBq/ml [^{131}I]NaI were set as negative controls. Radioactivity uptake of [^{131}I]NaI is measured as counts per minute per intracellular protein (CPM/mg).

In all experimental groups, the CPM/mg values increased as the [^{131}I]NaI uptake time increased from 0 to 10 minutes. In all experimental groups except 1.48 MBq/ml, the CPM/mg values decreased as the [^{131}I]NaI uptake time increased from 10 to 30 minutes. The CPM/mg values were relatively constant from 30 minutes to 60 min in all groups. Therefore, it is assumed that the [^{131}I]NaI concentration mediated by NIS becomes constant between 30 and 60 minutes and reaches saturation. When the uptake time was the same, CPM/mg values generally increased as the [^{131}I]NaI concentration increased. The rate of increase in CPM/mg was highest in the range of 1.48~4.44 MBq/ml and lowest in the range of 4.44~5.92 MBq/ml. No significant uptake activity was measured in HeLa cells that do not express NIS. Based on these results, the [^{131}I]NaI uptake time of 3D tumor spheroids were set to 30 minutes, and the [^{131}I]NaI concentration

of 3D tumor spheroids was set to 4.44 MBq/ml.

[^{131}I]NaI uptake was performed for 30 minutes, followed by clonogenic assays to investigate the biological effect of [^{131}I]NaI on cells(Figure 4B). HeLa cells showed no change in survival fraction regardless of the [^{131}I]NaI concentration. The survival fraction of HeLa-hNIS cells decreased with the [^{131}I]NaI concentration. The arithmetic increase in the [^{131}I]NaI concentration resulted in an exponential decrease in the survival fraction. These results statistically fit a linear-quadratic model (Table 1).

To calculate the biological equivalent absorbed dose, 0-8 Gy of external radiation was irradiated using ^{137}Cs, and chlorogenic analysis was performed (Figure 4C). The survival fraction of HeLa cells and HeLa-hNIS cells decreased with the absorbed dose. An arithmetic increase in the absorbed dose of both cells resulted in an exponential decrease in survival fraction. These results also statistically fit a linear-quadratic model (Table 1). The biological equivalent absorbed dose was calculated assuming that the survival fraction calculated from the linear quadratic model of [^{131}I]NaI uptake and the linear quadratic model of external irradiation in HeLa-hNIS cells were the same.

The biological equivalent absorbed dose of 4.44 MBq/ml [^{131}I]NaI uptake for 30 minutes is about 5.4 Gy. These results are summarized in Table 2.

(A)

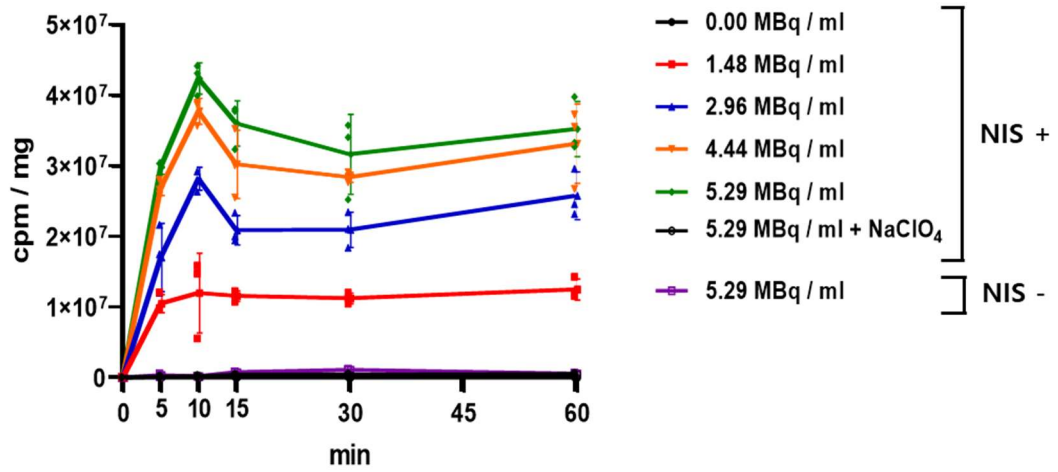
5×10^7
4×10^7
3×10^7
2×10^7
1×10^7
0
cpm / mg
0 5 10 15 30 45 60
min
0.00 MBq / ml
1.48 MBq / ml
2.96 MBq / ml
4.44 MBq / ml
5.29 MBq / ml
5.29 MBq / ml + NaClO4
NIS +
5.29 MBq / ml
NIS -

(B)

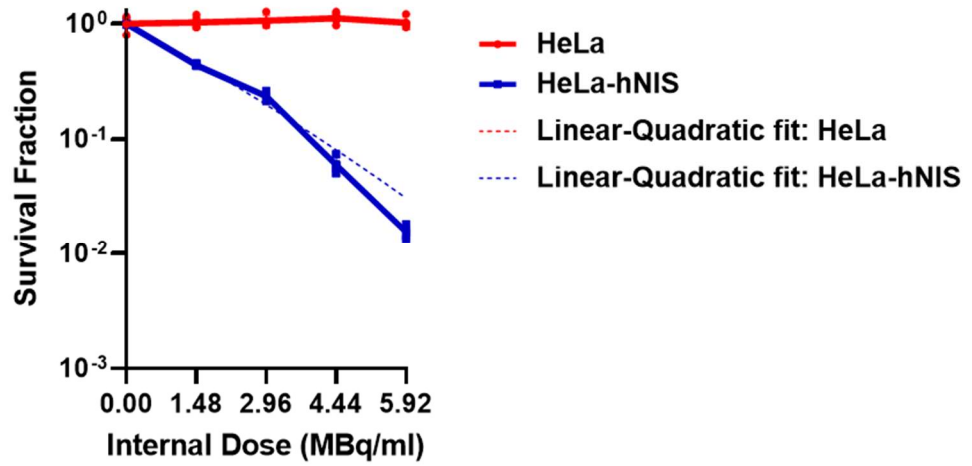
10^0
10^-1
10^-2
10^-3
Survival Fraction
0.00 1.48 2.96 4.44 5.92
Internal Dose (MBq/ml)
HeLa
HeLa-hNIS
Linear-Quadratic fit: HeLa
Linear-Quadratic fit: HeLa-hNIS

(C)

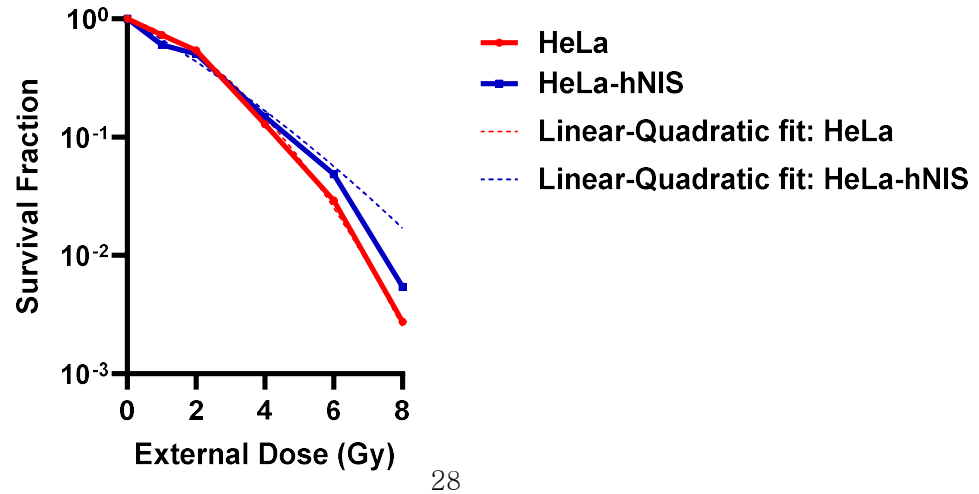
10^0
10^-1
10^-2
10^-3
Survival Fraction
0 2 4 6 8
External Dose (Gy)
HeLa
HeLa-hNIS
Linear-Quadratic fit: HeLa
Linear-Quadratic fit: HeLa-hNIS

Figure 4. Estimation of biological equivalent absorbed dose

(A) [^{131}I]NaI uptake dependent on [^{131}I]NaI concentration and uptake time in HeLa and HeLa/hNIS. Data represent mean ± SD (n = 4 per group); (B) Clonogenic survival analysis of [^{131}I]NaI uptake. Data represent mean ± SD (n = 4 per group); (C) Clonogenic survival analysis of external irradiation using ^{137}Cs.

Table 1. Comparison of linear quadratic models by radiation type and cell line

Radiation type	Cell line	α	β	α/β	Linear-quadratic model	R^2
[^{131}I]NaI uptake	HeLa	-0.0016	8.586×10^{-6}	-190.5	$SF = e^{0.0016D-8.586\times10^{-6}D^2}$	0.071
	HeLa-hNIS	0.0189	1.872×10^{-5}	1007	$SF = e^{-0.0189D-1.872\times10^{-5}D^2}$	0.994
External irradiation:^{137}Cs	HeLa	0.2025	0.0683	2.996	$SF = e^{-2025D-0.0683D^2}$	0.997
	HeLa-hNIS	0.3854	0.0154	24.97	$SF = e^{-3854D-0.0154D^2}$	0.987

Table 2. Conversion table of biological equivalent absorbed dose

[^{131}I]NaI concentration (MBq/ml)	Absorbed dose (Gy)	Survival fraction
0	0	1
1.48	1.89	0.4565
2.96	3.68	0.1964
4.44	5.40	0.0795
5.92	7.07	0.0303

Radioactivity distribution of [^{131}I]NaI in 3D tumor spheroids

[^{131}I]NaI uptake and efflux were measured in 3D tumor spheroids. The radioactivity distribution of [^{131}I]NaI absorbed inside the 3D tumor spheroids was analyzed. The radioactivity distribution was fitted to mathematical models, and the absorbed dose was calculated using the mathematical models. 3D tumor spheroids consisting of HeLa cells or HeLa-hNIS cells were treated with [^{131}I]NaI for 0.5 hour. Radioactivity uptake of [^{131}I]NaI in 3D tumor spheroids is measured as counts per minute per cell number in a 3D tumor spheroid (CPM/cell).

The radioactivity uptake of [^{131}I]NaI was significantly measured in only NIS-expressing 3D tumor spheroids compared to non-NIS-expressing 3D tumor spheroids (Figure 5A). The average CPM/cell values are 18-19(Figure 5B). A 3D tumor spheroid consists of approximately 7×10^4-1.5×10^5 cells. There was no significant correlation between the cell lines constituting the 3D tumor spheroids and the number of cells in the 3D tumor spheroids(Figure 5C).

The efflux time of [^{131}I]NaI in 3D tumor spheroids was measured. 50% of [^{131}I]NaI absorbed was released after 2.56 hours, and only 1% of [^{131}I]NaI remained in the cells after 16.60

hours (Figure 5D). Similar to the radioactive decay of radioactive isotopes, [^{131}I]NaI released from cells also decay exponentially. Fitting the data to an exponential decay function gives R^2 a value of 97.66. Based on this, the calculated residence time was 3.68 hours. These values were used for MIRDcell simulations.

(A)

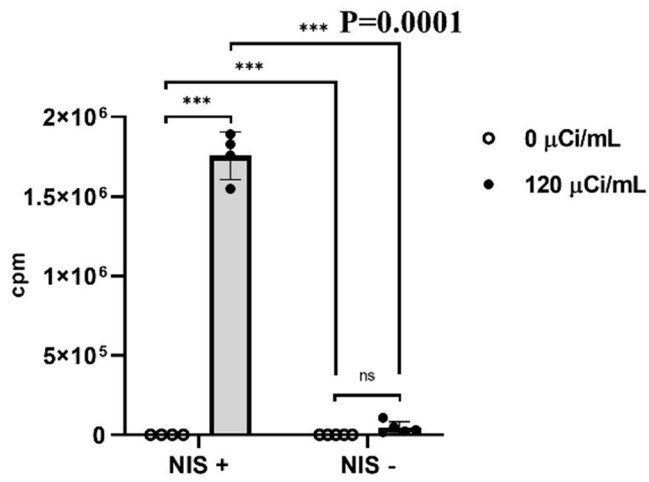
*** P=0.0001
***
***
2×10⁶
1.5×10⁶
1×10⁶
5×10⁵
0
cpm
ns
NIS +
NIS -
0 μCi/mL
120 μCi/mL

(B)

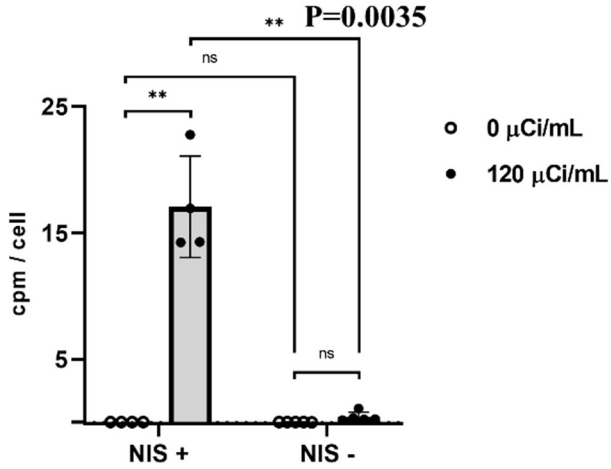
** P=0.0035
ns
**
25
15
5
cpm / cell
ns
NIS +
NIS -
0 μCi/mL
120 μCi/mL

(C)

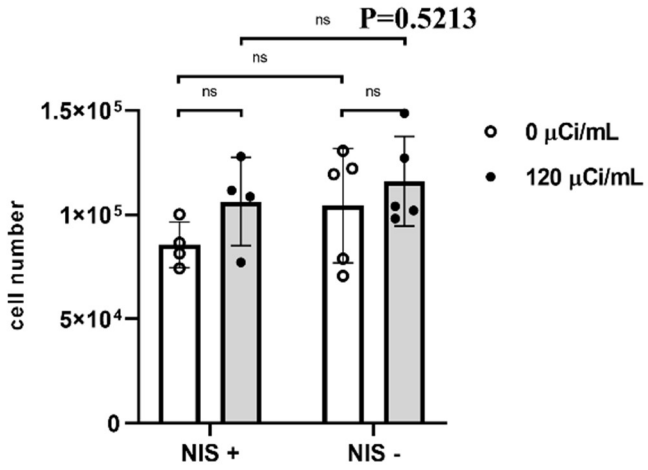
ns P=0.5213
ns
ns
ns
1.5×10⁵
1×10⁵
5×10⁴
0
cell number
NIS +
NIS -
0 μCi/mL
120 μCi/mL

(D)

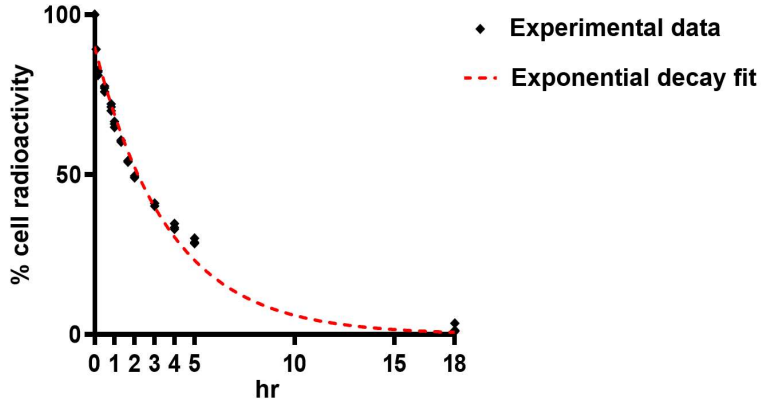

Figure 5. [^{131}I]NaI uptake and efflux in 3D tumor spheroids consist of HeLa cells or HeLa-hNIS cells

(A) Total radioactivity absorbed by 3D tumor spheroid; (B) Radioactivity per cell in 3D tumor spheroids; (C) Numbers of cells in one 3D tumor spheroid; The number of cells that consist of a spheroid is also related to the size of the spheroid. All data from [^{131}I]NaI uptake assay in 3D tumor spheroids represent mean ± SD (n = 5 per group); (D) % radioactivity released by 3D tumor spheroid. Data from [^{131}I]NaI efflux assay in 3D tumor spheroids represent mean ± SD (n = 3 per group);

To analyze the radioactivity distribution of [^{131}I]NaI in 3D tumor spheroids, 3D tumor spheroids were sequentially dissociated using a cell dissociation reagent. After adding the cell dissociation reagent, cell dissociation from outside the 3D tumor spheroid was observed using bright-field microscopy (Figure 6A). Dissociated cells were obtained to measure radioactivity, and the number of cells was counted. Assuming the diameter of a cell and inversely calculating the size of a 3D tumor spheroid based on cell number, the radius of a 3D tumor spheroid is approximately 700-800 μm. This is analogous to the radius of a 3D tumor spheroid observed under bright-field microscopy.

The '% radioactivity/cell of [^{131}I]NaI uptake' versus 'distance from the center of the 3D tumor spheroid' was plotted as a radial distribution graph. In a 3D tumor spheroid with a radius of 750 μm, more than 80% of %activity/cell was distributed more than 500 μm away from the center of the 3D tumor spheroid (Figure 6B). Converted to percentage, more than 80% of %activity/cell were distributed in the outer 35% of the diameter (Figure 6C). In Figure 6D, the radial distribution of '% radioactivity/cell' versus 'distance from the center of the 3D tumor spheroid' is merged with the Fucci image of the 3D tumor spheroid.

(A)

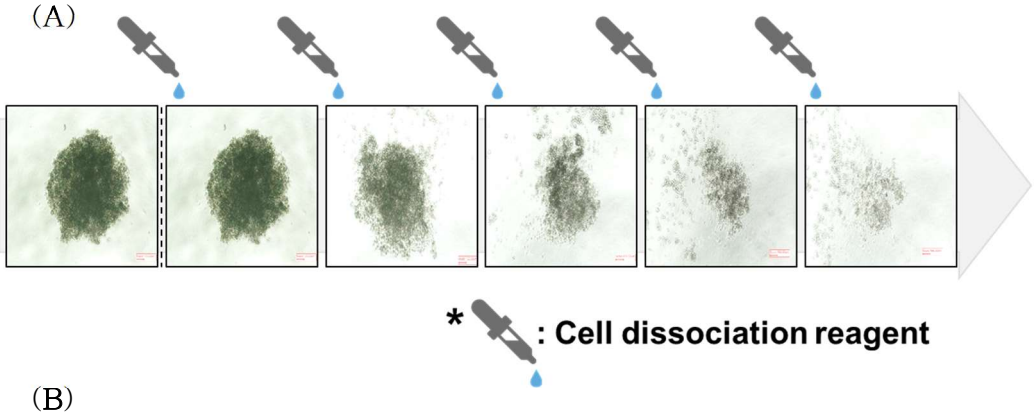
* : Cell dissociation reagent

(B)

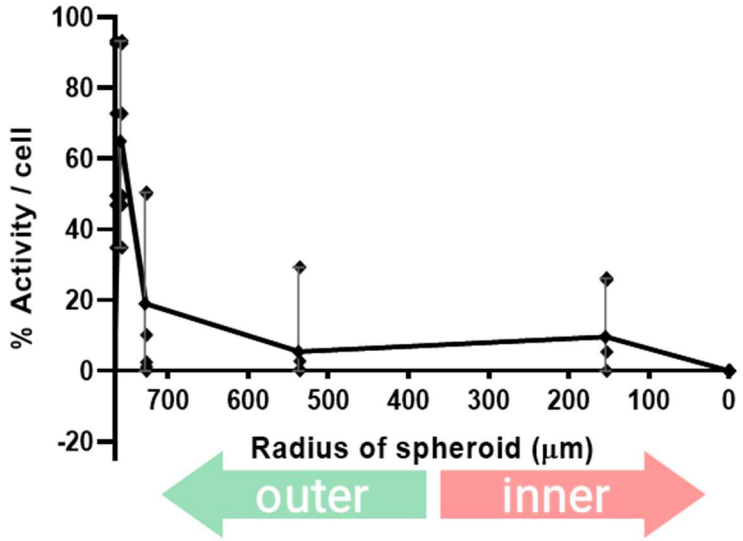
% Activity / cell
100
80
60
40
20
0
-20
700
600
500
400
300
200
100
0
Radius of spheroid (μm)
outer
inner

(C)

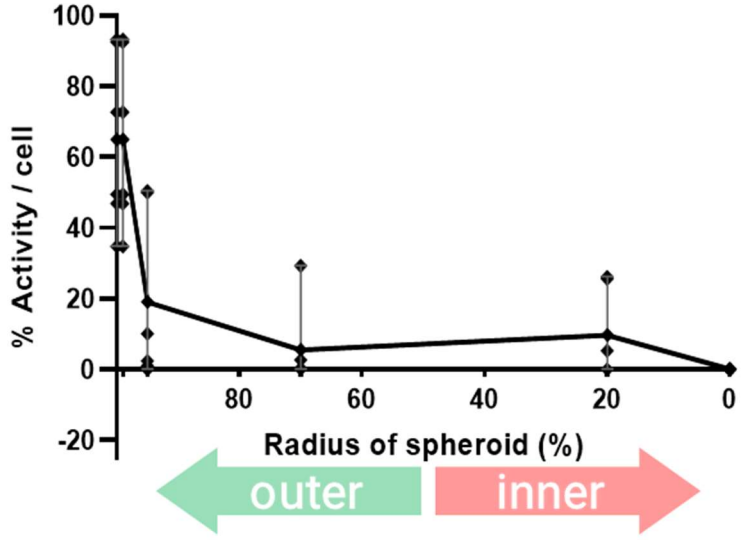
% Activity / cell
100
80
60
40
20
0
-20
80
60
40
20
0
Radius of spheroid (%)
outer
inner

(D)

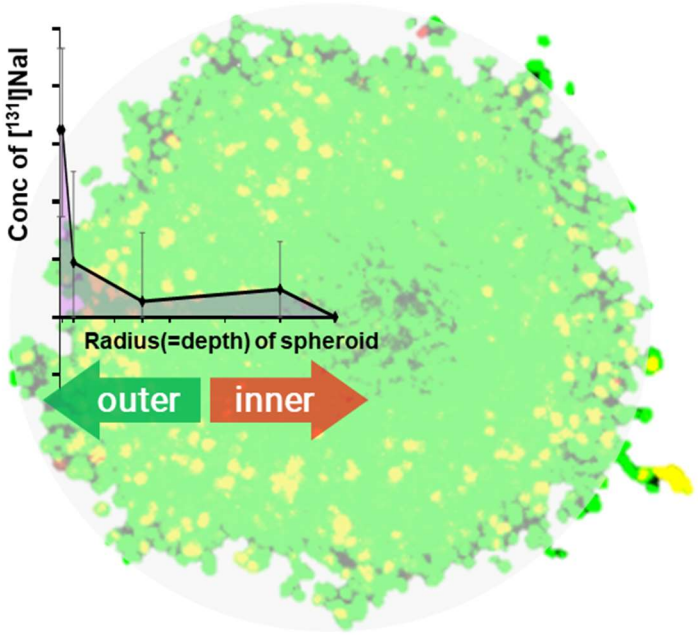

Figure 6. Radioactivity distribution of [^{131}I]NaI in 3D tumor spheroids

(A) Cell dissociation image of the 3D tumor spheroid. The radius of 3D tumor spheroids is approximately 750 μm; (B) Radial distribution of the '% radioactivity/cell' versus 'distance from the center of the 3D tumor spheroid'. Data represent mean ± SD (n = 5 per group); (C) Radial distribution of the '% radioactivity/cell' versus '% distance from the center of the 3D tumor spheroid'. Data represent mean ± SD (n = 5 per group); (D) Fucci image of the 3D tumor spheroid merged with the radial distribution of '% radioactivity/cell' versus 'distance from the center of the 3D tumor spheroid'

The radial distribution of '%activity/cell' versus '%distance from the centroid of the 3D tumor spheroid' was fitted with a lognormal, cubic polynomial, quadratic polynomial, and linear (Figure 7). The goodness of fit was evaluated by comparing the R^2 values of the fitted model. As a result, The R^2 values of the fit equation were high in the order of the lognormal, cubic polynomial, quadratic polynomial, and linear. In general, the more coefficients (parameters) in the fitting equation, the better the fit to the data. The R^2 value lognormal model was approximately 0.68 (Figure 7A). The lognormal model was suitable for radioactivity distributed outside the 3D tumor spheroid, especially for the '% distance from 3D tumor spheroid centroid' of >80%. The R^2 value of the cubic polynomial model was approximately 0.60 (Figure 7B). The cubic polynomial model was suitable for the activity distributed inside the 3D tumor spheroid, especially for the '% distance from the center of 3D tumor spheroid' of < 20%. The R^2 value of the quadratic polynomial model was about 0.51 (Figure 7C). The R^2 value of the linear model was about 0.39, which hardly reflects the radioactivity distribution of the 3D tumor spheroid (Figure 7D). The best-fit equations and R^2 value are shown in Table 3. Thus, the absorbed dose to cells and cell

survival response were simulated based on the lognormal distribution model.

(A)

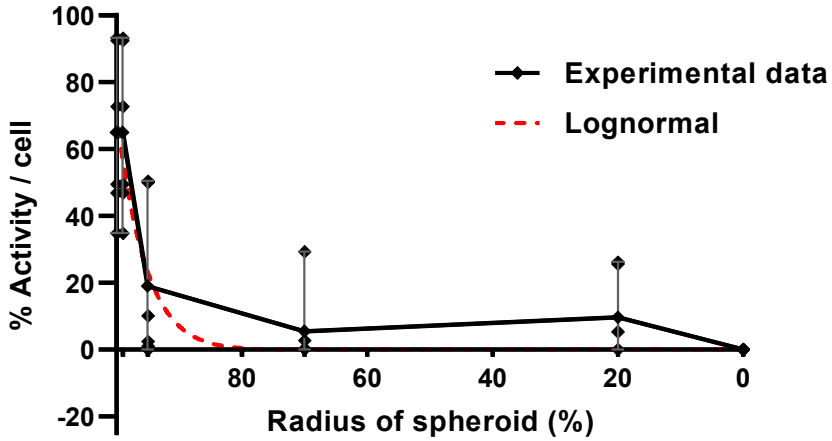
100
80
60
40
20
0
-20
% Activity / cell
80
60
40
20
0
Radius of spheroid (%)
Experimental data
Lognormal

(B)

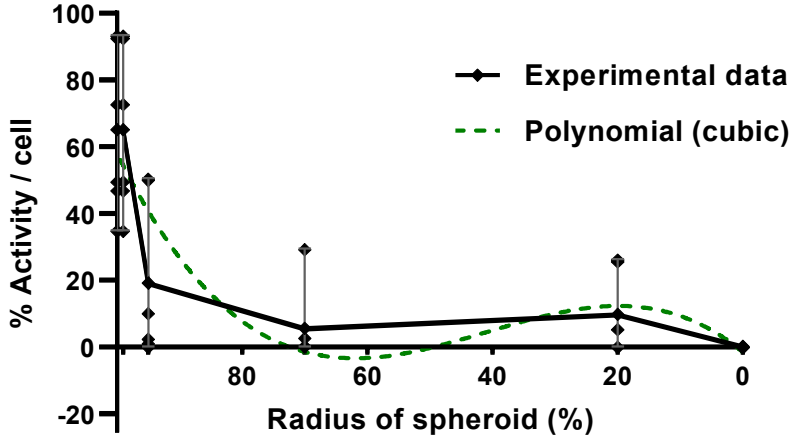
100
80
60
40
20
0
-20
% Activity / cell
80
60
40
20
0
Radius of spheroid (%)
Experimental data
Polynomial (cubic)

(C)

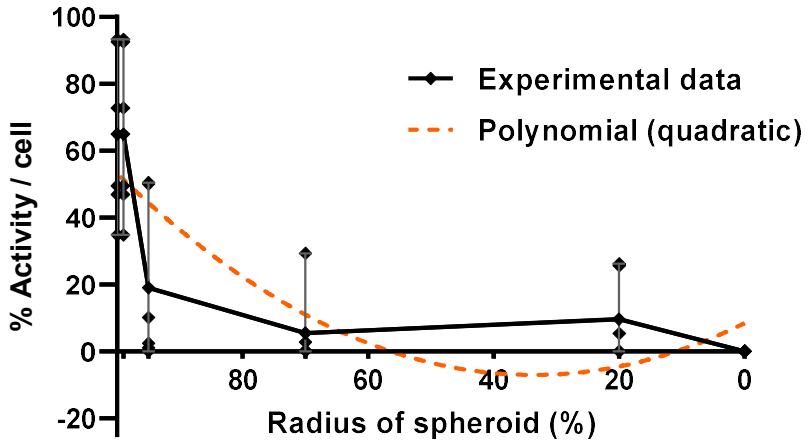
100
80
60
40
20
0
-20
% Activity / cell
80
60
40
20
0
Radius of spheroid (%)
Experimental data
Polynomial (quadratic)

(D)

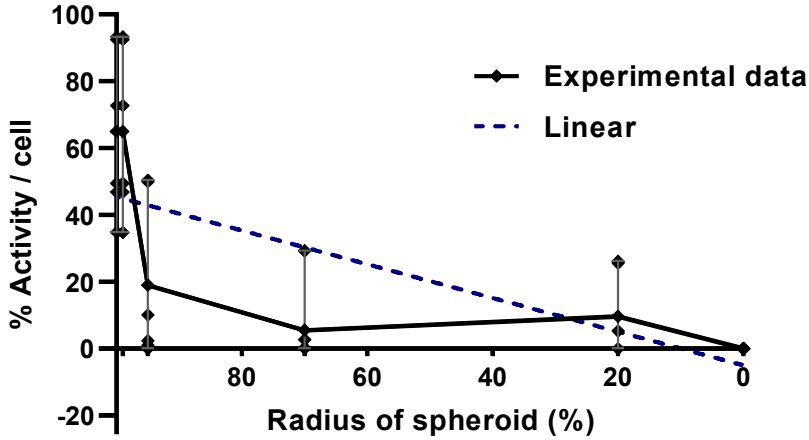
100
80
60
40
20
0
-20
% Activity / cell
80
60
40
20
0
Radius of spheroid (%)
Experimental data
Linear

Figure 7. Mathematical curve fitting of radioactivity distribution

Mathematical curve fitting for radioactivity distribution with [^{131}I]NaI in 3D tumor spheroids; (A) lognormal curve, (B) cubic polynomial, (C) quadratic polynomial curve, and (D) linear curve for radioactivity distribution of spheroids depth. Data represent mean ± SD (n = 5 per group).

Table 3. Best fitting equation of radioactivity distribution

	Fitting equation	R^2
Lognormal	$\%A = \frac{3.446x1019}{\%r} \exp\left(-0.5\left(\frac{\ln\left(\frac{\%r}{2497}\right)}{\ln(1.46)}\right)^2\right)$	0.6758
Cubic polynomial	$\%A = 0.0004206 \cdot \%r^3 - 0.05162 \cdot \%r^2 + 1.553 \cdot \%r - 1.302$	0.6034
Quadratic polynomial	$\%A = 0.01367 \cdot \%r^2 - 0.9197 \cdot \%r - 8.439$	0.5097
Linear	$\%A = 0.5041 \cdot \%r - 7.167$	0.3897

%A : %activity / cell
%r : %radius of 3D tumor spheroid

MIRDcell simulation of absorbed dose and cell survival response to cells in 3D tumor spheroids

The fitting model derived from the experiment was input into MIRDcell. 3D cell clusters of similar size to experimental 3D tumor spheroids were modeled. Absorbed dose and cell survival response were simulated by changing various parameters. Some parameters are derived from experiments, and others are referenced from existing studies. The 'max mean activity per cell' was determined to be 0.4 Bq.

1. Distribution of radioactivity

The absorbed dose at the center of the spheroid was low in the order of lognormal distribution, cubic polynomial distribution, quadratic polynomial distribution, and linear distribution (Figure 8). The 'mean absorbed dose to cell' was proportional to the 'max mean activity per cell.' Although most of the ^{131}I activity uptake was concentrated outside the 3D tumor spheroid in the experiment, some radioactivity was distributed inside the 3D tumor spheroid in the cubic polynomial, quadratic polynomial, and linear models, except for the lognormal distribution. Regardless of the radioactivity distribution model, the absorbed dose range

to cells was much more comprehensive than that of radioactivity distribution. Radioactivity distribution and mean absorbed dose to cell do not correspond. The absorbed dose was the lowest in the linear model despite the highest radioactivity distribution outside the spheroid. The maximum absorbed dose ranged from 50 Gy to 2600 Gy. It was tens to hundreds of times higher than the radiation in clinical studies. Due to high absorbed doses, all cells in the 3D tumor spheroid were predicted to die regardless of the distribution model.

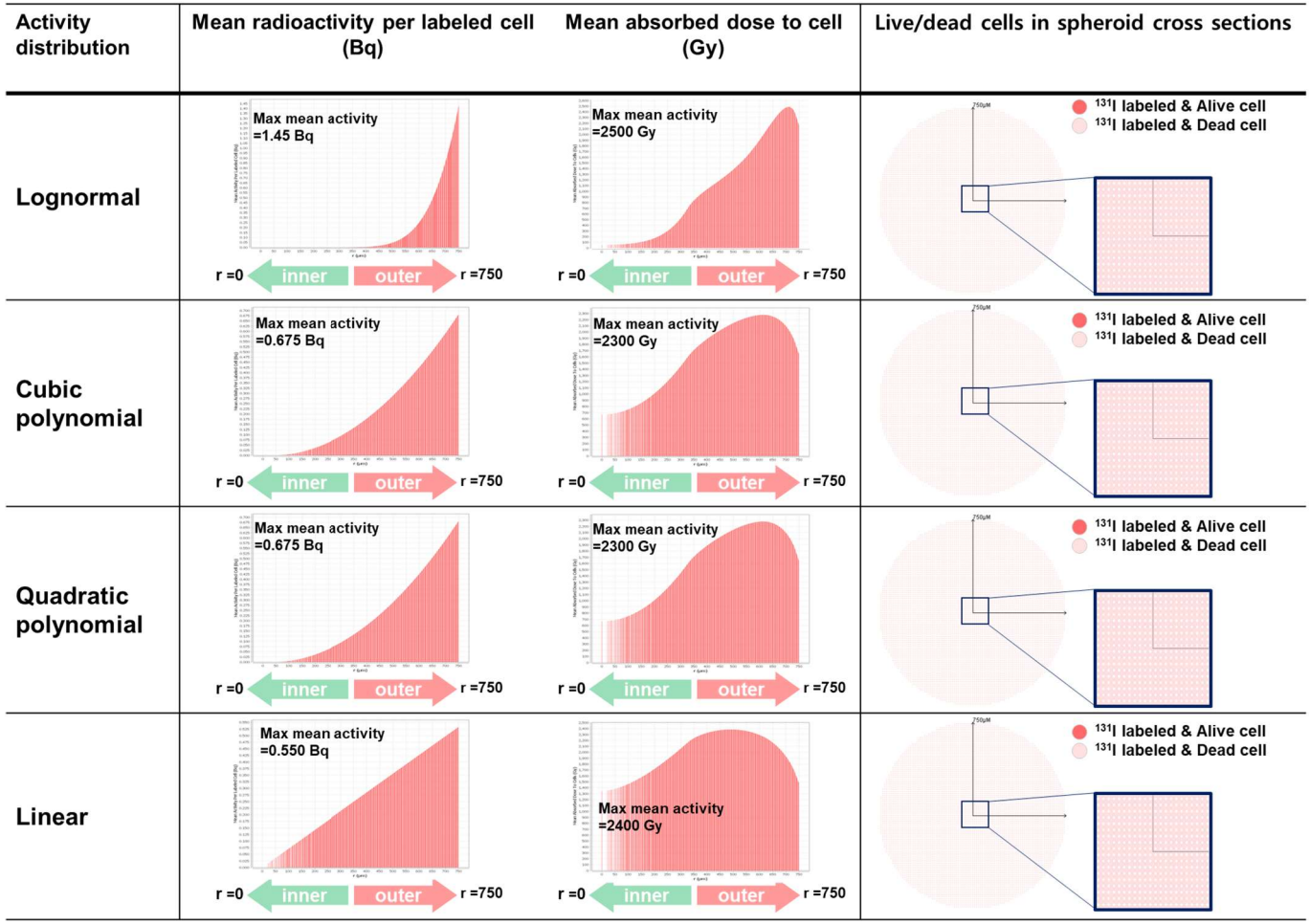

Figure 8. Mean absorbed dose and survival response for radial distribution calculated by MIRDcell: depending on the type of radiation distribution model

2. Type of radionuclide

When using radiopharmaceuticals, the activity of the radiopharmaceuticals varies depending on the radiation emitted. However, in this study, the 'max mean activity per cell' was set constant regardless of the radionuclide. (Figure 9). The absorbed dose of ^{211}At, which emits α-rays, is much narrower and 3.8 times higher than the absorbed dose of ^{131}I. Unlike ^{131}I, the absorbed dose range of ^{211}At generally corresponds to radioactivity distribution. Despite the high ionization energy of α-ray, cell survival was predicted in the central region of the 3D tumor spheroid with no absorbed dose. ^{123}I, which emits gamma rays, showed almost the same absorbed dose range and radioactivity distribution despite the characteristics of γ-rays with a wide penetrating range. The maximum absorbed dose of ^{123}I was about 16% lower than that of ^{131}I. Likewise, alive cells were distributed in the region where the absorbed dose of ^{123}I was low. The absorbed dose ranges of ^{211}At and ^{123}I were almost identical, but the percentage of viable cells was higher in ^{123}I.

Radionuclide	Mean radioactivity per labeled cell (Bq)	Mean absorbed dose to cell (Gy)	Live/dead cells in spheroid cross sections
^{131}I β⁻ : 90% (606 keV) γ : 81% (364 keV)	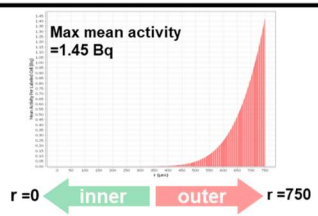	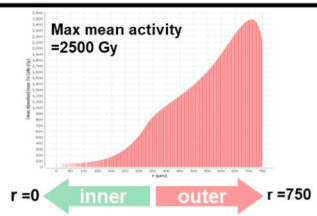	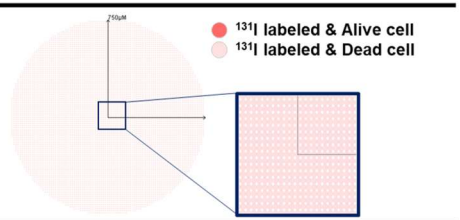
^{211}At α : 58% (7500 keV)	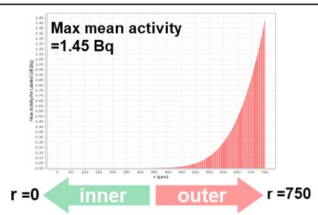	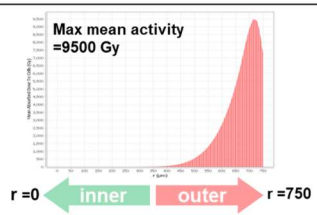	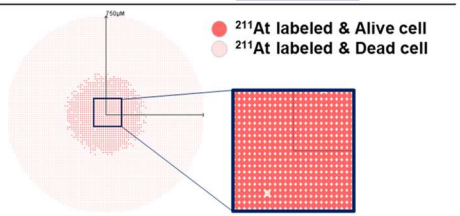
^{123}I EC : 100% (159 keV)	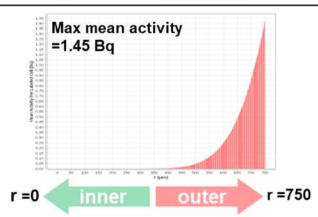	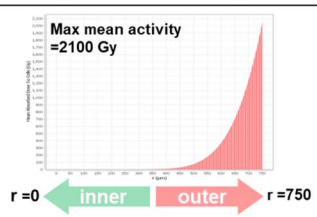	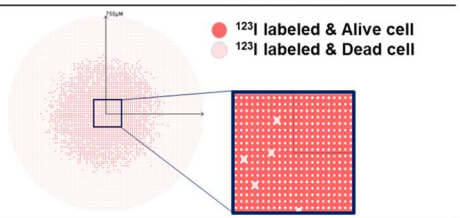

Figure 9. Mean absorbed dose and survival response for radial distribution calculated by MIRDcell: depending on the type of radionuclide

4. Time-integrated activity coefficient

In MIRD formalism, the time-integrated activity coefficient is proportional to cumulative activity. In this simulation, the average absorbed dose to cells increased or decreased proportionally to the time-integrated radioactivity coefficient (Figure 10). With a time-integrated radioactivity coefficient of 277.77 hours, the maximum mean absorbed dose is 2500 Gy. The absorbed dose was too high for the cells to survive.

Time-integrated activity coefficient is a parameter for approximating the decay of radionuclides under the assumption that the radionuclide remains indefinitely in cells. Since actual radionuclides do not remain in cells indefinitely, a time-integrated radioactivity coefficient has been substituted by the biological residence time calculated from the iodine efflux assay. With a time-integrated radioactivity coefficient of 3.68 hours, the maximum mean absorbed dose to cells was 33.75 Gy. It was predicted that alive cells would exist in the region where the absorbed dose was 10 Gy or less.

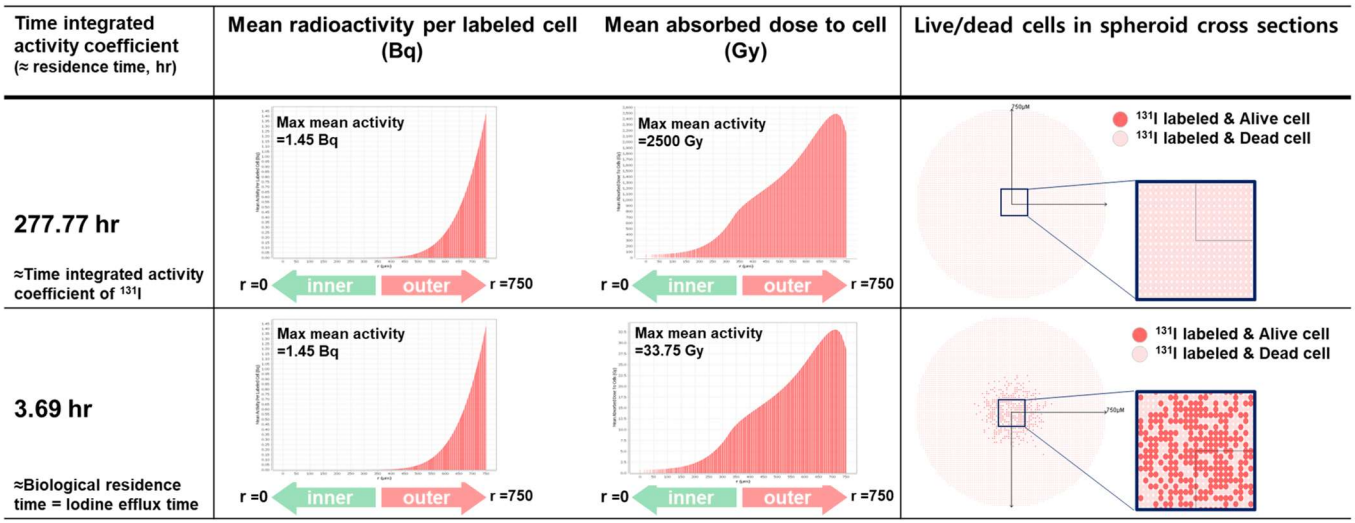

Figure 10. Mean absorbed dose and survival response for radial distribution calculated by MIRDcell: depending on the time-integrated activity coefficient

5. Proportion of radionuclide (^{131}I)-labeled cells

When a random mixture of ^{131}I-labeled and ^{131}I-unlabeled cells was distributed on 3D tumor spheroids, the mean absorbed dose to the cells, and the cell survival response was simulated (Figure 11). They resemble 3D tumor spheroids formed by a mixture of NIS-expressing and non-NIS-expressing cells. When a random mix of ^{131}I-labeled and non-^{131}I-labeled cells was distributed on 3D tumor spheroids, the average absorbed dose and cell survival response to cells were simulated (Figure 11).

As a result of the simulation, the maximum value of the mean absorbed dose was proportional to the decrease in ^{131}I-labeled cells. When the ^{131}I-labeled cells decrease from 100% to 50%, the maximum value of the mean absorbed dose also reduces by half. The shape of the mean absorbed dose histogram for cells was constant. When the number of ^{131}I-labeled cells was 25% or more, all ^{131}I-labeled cells were killed by the absorbed dose emitted from ^{131}I-labeled cells. When ^{131}I-labeled cells were 5%, less than 10% of ^{131}I-unlabeled and ^{131}I-labeled cells survived in the center of 3D tumor spheroids. Cell survival fraction decreased as the number of cells labeled with ^{131}I increased, but

labeled cells did not die significantly more than ^{131}I-unlabeled cells.

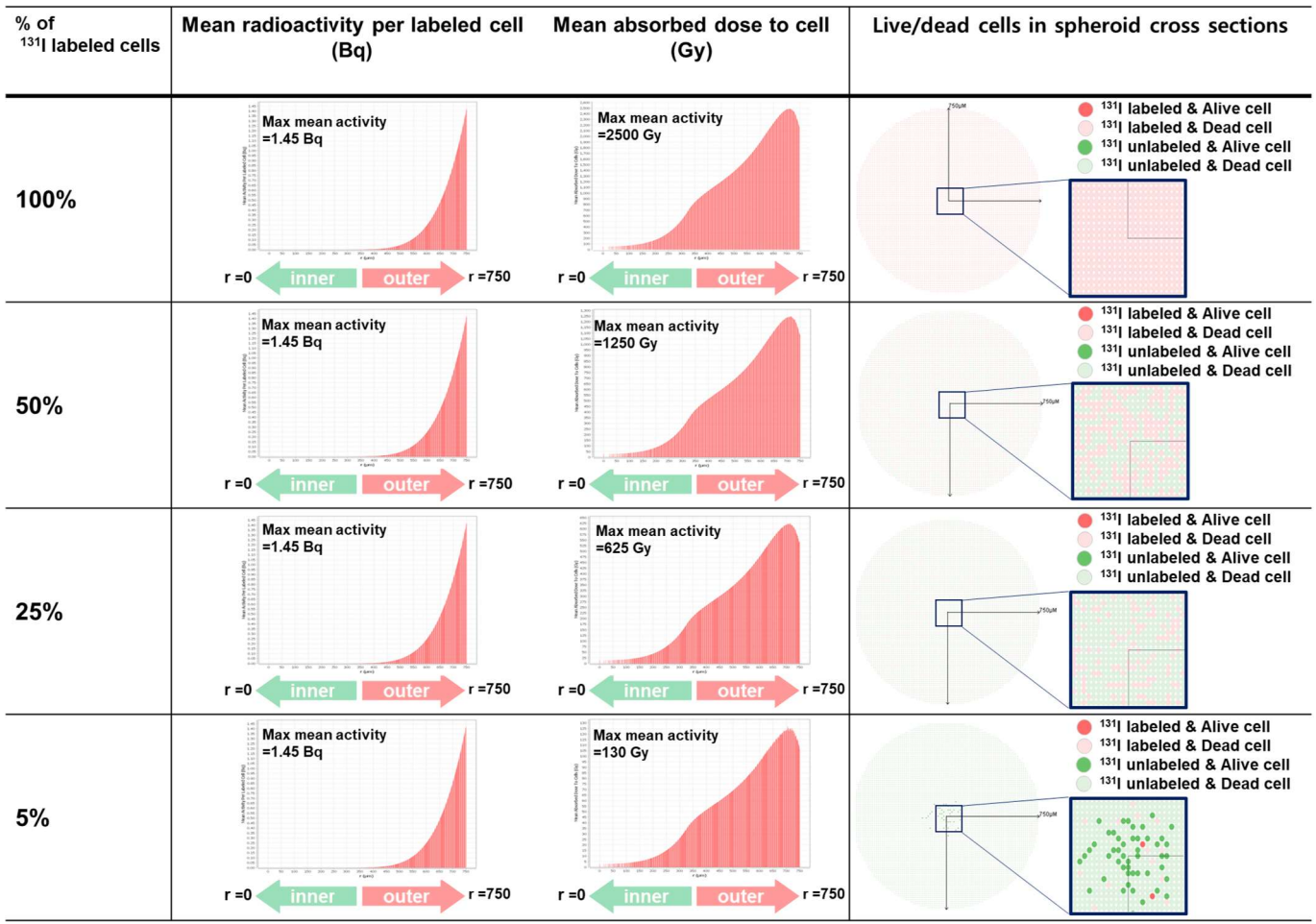

Figure 11. Mean absorbed dose and survival response for radial distribution calculated by MIRDcell: depending on the proportion of ^{131}I–labeled cells

Induced cell cycle arrest with [^{131}I]NaI uptake in 3D tumor spheroids

Continuous cell cycle analysis allowed evaluation of relative differences in cellular response and damage repair to radiation dose. The cell cycle was analyzed using Fucci expressed in cells.

3D tumor spheroids consisting of HeLa-Fucci cells or HeLa-Fucci/hNIS cells were treated with [^{131}I]NaI for 30 minutes, then the fluorescence of the 3D tumor spheroids was monitored at 6 hours intervals for 24 hours.

3D tumor spheroids consisting of HeLa-Fucci cells showed no significant fluorescence change after [^{131}I]NaI treatment (Figure 12A). That is, the cell cycle continued. As a result of quantitative analysis of fluorescence distribution, there was no significant difference in the ratio of red(G_1) fluorescence to green($S-G_2-M$) fluorescence (Figure 12B). As the 3D tumor spheroid cells proliferated, the fluorescence regions increased over time. Although whole fluorescent areas in the 3D tumor spheroid were normalized, there was no difference in the red(G_1) ratio to green($S-G_2-M$) fluorescence.

In 3D tumor spheroids consisting of HeLa-Fucci/hNIS cells, red(G_1) fluorescence rapidly decreased in the whole region of

the 3D tumor spheroid after 6 hours of [^{131}I]NaI treatment (Figure 12C). That is, the cell cycle is arrested before the G_1 phase. Over time, the cell cycle of some cells resumes. As a result of quantitative analysis of the fluorescence distribution, the red(G_1) fluorescence ratio rapidly decreased, and the ratio of ($S-G_2-M$) fluorescence slightly increased. (Figure 12D). The fluorescence region dropped after 6 hours of [^{131}I]NaI treatment. As the cells in the 3D tumor spheroid proliferated, some cells progressed through the cell cycle, and the whole fluorescence region in the 3D tumor spheroid increased again over time. Decreases in red(G_1) and increases in green($S-G_2-M$) fluorescence are shown on a normalized graph of the fluorescence region of 3D tumor spheroids.

(A)

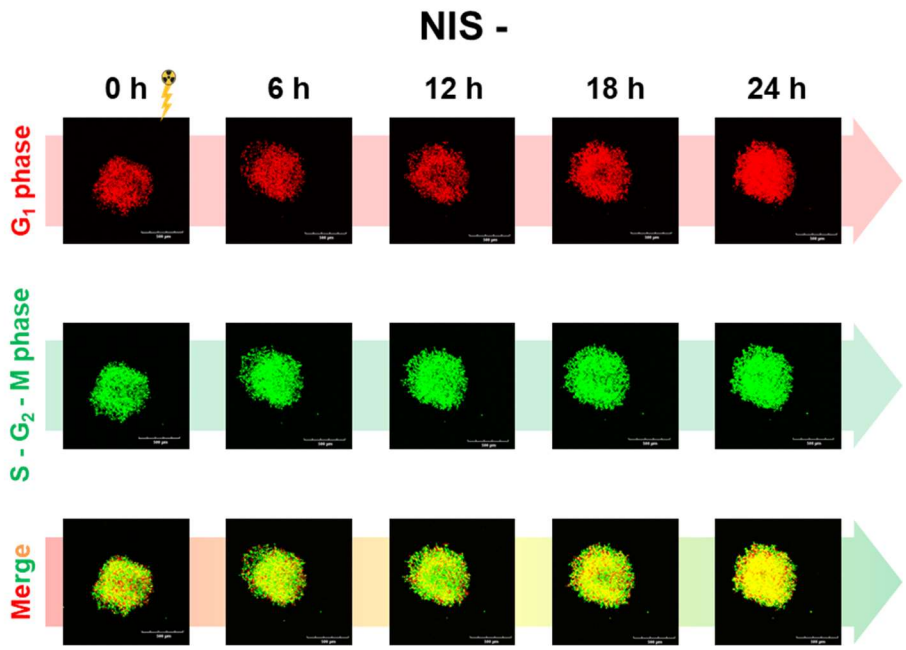
NIS -
0 h
6 h
12 h
18 h
24 h
G1 phase
S - G2 - M phase
Merge

(B)

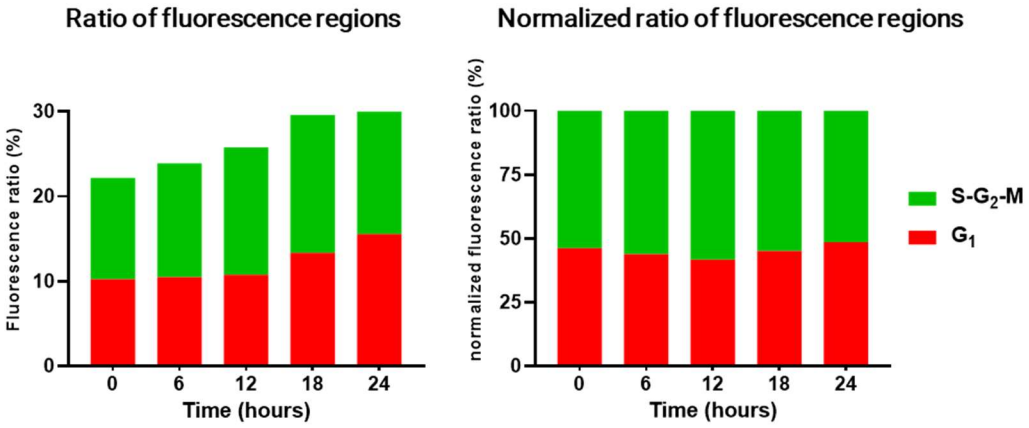
Ratio of fluorescence regions
Fluorescence ratio (%)
30
20
10
0
0
6
12
18
24
Time (hours)
Normalized ratio of fluorescence regions
normalized fluorescence ratio (%)
100
75
50
25
0
0
6
12
18
24
Time (hours)
S-G2-M
G1

(C)

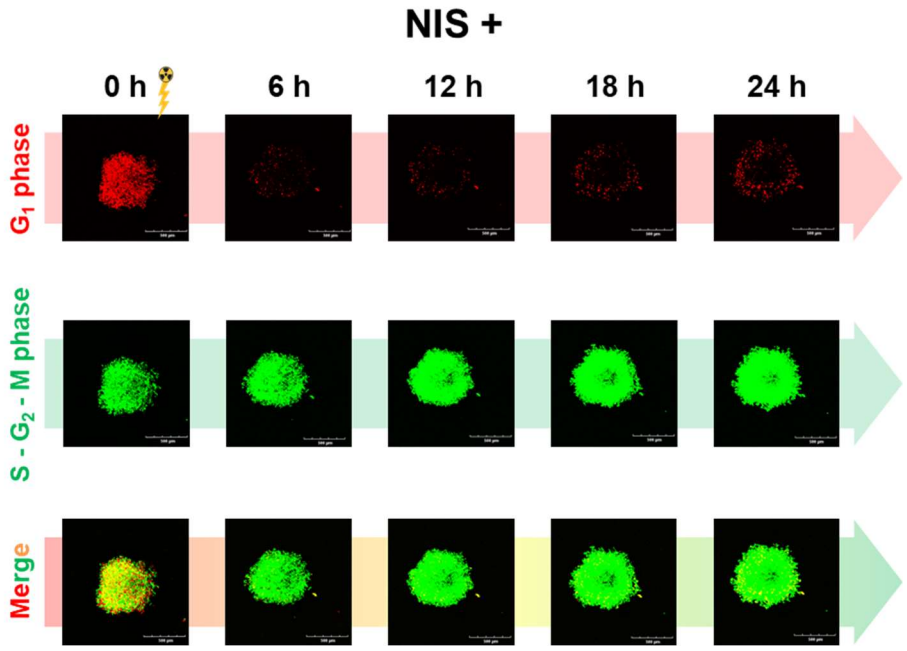
NIS +
0 h
6 h
12 h
18 h
24 h
G1 phase
S - G2 - M phase
Merge

(D)

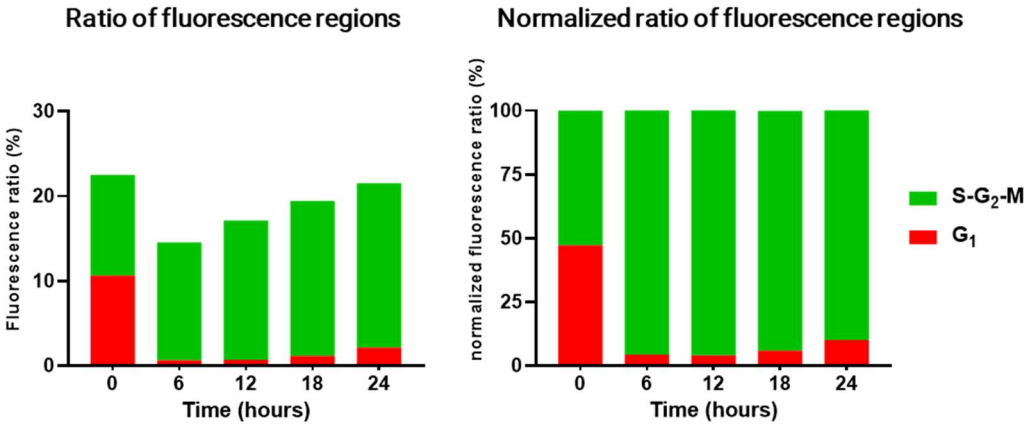
Ratio of fluorescence regions
Fluorescence ratio (%)
30
20
10
0
0
6
12
18
24
Time (hours)
Normalized ratio of fluorescence regions
normalized fluorescence ratio (%)
100
75
50
25
0
0
6
12
18
24
Time (hours)
S-G2-M
G1

Figure 12. Induced cell cycle arrest with [^{131}I]NaI uptake in 3D tumor spheroids.

(**A**) Live imaging of cell cycle with [^{131}I]NaI using confocal microscopy imaging for 24 hours in the spheroid of HeLa; (**B**) Percentage of fluorescence ratio and (**C**) Normalized fluorescence ratio between S−G_2−M and G_1 phase at each time points (0, 6, 12, 18 and 24 hours) in the spheroid of HeLa. (**D**) Live imaging of cell cycle with [^{131}I]NaI using confocal microscopy imaging for 24 hours in the spheroid of HeLa/hNIS. (**E**) Percentage of fluorescence ratio and (**F**) Normalized fluorescence ratio between S−G_2−M and G_1 phase at each time point (0, 6, 12, 18, and 24 hours) in the spheroid of HeLa/hNIS.

DISCUSSION

Compared to the history and diversity of radiopharmaceutical therapy, the lack of basic research on radiopharmaceuticals is due to the complexity of radiopharmaceutical therapy(15-20). Numerous physical and biological variables are considered in treatment planning and outcome prediction of radiopharmaceutical therapy. Therefore, a preclinical model is required to calculate and study various variables in radiopharmaceutical therapy. In this study, various variables considered in radiopharmaceutical therapy were simulated using 3D tumor spheroids, and the possibilities and limitations of 3D tumor spheroids for radiopharmaceutical research were evaluated.

The 3D tumor spheroid model is one of the previously presented preclinical models(5-8). 3D tumor spheroids with tumor-like physical structures are simple to generate, experimental conditions can be easily controlled, and various radiation delivery methods can be experimented with(6). In this study, the sodium iodide symporter was expressed in cells using a viral vector to deliver radioactive iodine ^{131}I into cells. In addition to NIS, 3D tumor spheroids can be used to evaluate various radionuclide

delivery methods, such as small molecules, peptides, antibodies, nanostructures, and microspheres.

A key aspect of radiopharmaceutical treatment strategies is predicting and evaluating target cells' response to radiation(1-4). To this end, it is necessary to measure the absorbed dose of radiation emitted by the radiopharmaceutical reaching the cell and to calculate the effect of the absorbed dose on the cell. Accurate absorbed dose measurements are complicated when there is more than one emitter and absorber(11-13). The most widely recognized method for assessing the biological effects of radiation on cells is to measure cell survival fraction using clonogenic assays(1, 5). In this study, ^{137}Cs γ-ray irradiation, which can adjust the absorbed dose, and [^{131}I]NaI uptake experiment, which can calculate the radioactivity concentration, were performed in parallel to calculate the absorbed dose required to induce the cell survival response uniformly. Although the biological equivalent absorbed dose can be calculated easily and intuitively, this experimental method has some limitations. First, the difference in radiation was not considered. β-rays from ^{131}I and γ-rays from ^{137}Cs have different ionization energies. However, this type of radiation was not considered, and the

therapeutic effect of β-rays was estimated from the absorbed dose of γ-rays. Second, it is impossible to distinguish whether the therapeutic effect of ^{131}I is due to intracellular uptake of [^{131}I]NaI or the radiation of [^{131}I]NaI distributed extracellularly. Similarly, the absorbed dose is not uniform because [^{131}I]NaI uptake depends on intracellular biological factors. Although Neti P.V. et al. experimentally verified the isolating effects of microscopic nonuniform distributions of ^{131}I on labeled and unlabeled cells, it is still incomplete(21).

A multicellular dosimetry program was used to overcome the limitations of these experiments. Several multicellular dosimetry programs have been developed that use Monte Carlo simulations based on particle transport codes and MIRD formalities to calculate complex absorbed doses and biological responses(11-13). This multicellular dosimetry program, like MIRDcell, COOLER, and PARaDIM, can model complex biological responses based on experimentally determined biological parameters(9). By revalidating these modeled biological responses in 3D tumor spheroids, complex parameters of radiopharmaceutical therapy can be understood and evaluated.

As primary data for multicellular dosimetry and modeling, the radial distribution of radiopharmaceuticals was measured in 3D tumor spheroids. 80% of the radioactivity was distributed in the outer 35% of the 3D tumor spheroid. The radioactivity of ^{131}I versus distance from the center of a 3D tumor spheroid was fitted with a lognormal curve. Although it has already been suggested that cellular uptake of radioactivity follows a lognormal distribution, few studies have directly measured and validated uptake activity experimentally(22,23). In this study, 3D tumor spheroids were sequentially dissociated to analyze radioactivity distribution instantly. Absorbed dose and cellular response by radiopharmaceutical treatment were modeled using MIRDcell. The survival response values obtained from the clonogenic assay experiment were entered, and the geometric information of the 3D tumor spheroid, the lognormal distribution of activity, and the maximum value of mean activity measured in single cells were entered. The time-integrated activity coefficient, the ratio of radionuclide-labeled/unlabeled cells, and the average energy spectrum of radionuclide (^{131}I) were calculated using the values set in the program. As a result of the simulation, when the max mean activity per cell was 0.4 Bq, the

max mean absorbed dose was 2500 Gy, and all cells died. Considering that the radiation in clinical therapy is partial radiation of less than 100 Gy, this is a too high number. Under the assumption that there is no error in the program, simulation analysis was performed by changing parameters such as radioactivity distribution, radionuclide, time-integrated radioactivity coefficient, and radionuclide labeled/unlabeled cell ratio. The type of radioactivity distribution had a significant effect on the average absorbed dose at the center of the spheroid. Linearly distributed radioactivity has an absorbed dose more than ten times higher than lognormally distributed radioactivity, even if the maximum mean radioactivity per cell is the same. As a result of the radionuclide was changed, the average absorbed dose of each radionuclide was highest for ^{211}At and lowest for ^{123}I. Nevertheless, ^{131}I's cell survival rate was the lowest. This is due to the difference in penetration range. Alpha rays from ^{211}At have high ionization energy and a narrow penetration range. The gamma rays from ^{123}I have an extensive penetrating range and lack the ionizing energy required for cell death. Beta rays emitted from ^{131}I have enough energy to kill cells. The penetration range of the beta ray is larger than the diameter of

the 3D tumor spheroid. If the maximum average radioactivity per cell was constant, the penetration range affected the survival response more than the max mean absorbed dose to cells. A lot of information can be inferred from changes in time-integrated activity coefficients. Since the time-integrated radioactivity coefficient is proportional to the accumulated radioactivity, the smaller the time-integrated radioactivity coefficient, the lower the absorbed dose and the higher the cell survival fraction. When the max mean activity per cell was 0.4 Bq, if the remaining time of intracellular iodine is experimentally measured and substituted into the time-integrated radioactivity coefficient, the max mean absorbed dose to cells is 33.75 Gy and the cell survival fraction is about 10%. Considering that the time-integrated radioactivity coefficient in the MIRD formalism is a parameter for approximating the decay of radionuclides under the assumption that radionuclides remain in the body indefinitely, modifications are required to introduce the time-integrated radioactivity coefficient(3,15,18). In clinical radiopharmaceutical therapy, some radiopharmaceuticals bind to cellular targets when radiopharmaceuticals are administered into the body. Unbound or dissociated radiopharmaceuticals are not immediately excreted

from the body. They are passed through the kidneys over several days after circulating in the body along blood vessels or lymphatics. Meanwhile, in the preclinical radiopharmaceutical test, the cell surfaces are exposed for several minutes to several hours to bind the radiopharmaceutical to the intracellular target(3,15,18). The radiopharmaceutical attached to the cell target is dissociated again within a short time, and the radiopharmaceutical released outside the cell is immediately removed when the culture medium is replaced. Considering this mechanism, it is necessary to experimentally calculate and use the time-integrated radioactivity coefficient considering the release time of radiopharmaceuticals from cells rather than the time-integrated radioactivity coefficient based on the decay of radionuclides in preclinical studies.

The change in the ratio of radionuclide-labeled cells to unlabeled cells also showed significant results. As the proportion of radionuclide-labeled cells decreased, the absorbed dose decreased, and the cell survival fraction increased. Because different cells have different target expressions, the ratio of radionuclide-labeled and unlabeled cells must be adjusted experimentally(21). To validate these MIRDcell simulation

results, experiments are required to construct 3D tumor spheroids by dividing the percentage of cells that uptake ^{131}I and those that do not uptake ^{131}I and evaluate the cellular response to ^{131}I.

The range of absorbed doses was much more comprehensive than the radioactivity distribution. Radiation was absorbed even in the 3D tumor spheroid region where ^{131}I did not exist. To determine the effect of absorbed dose on cells, radiation-induced cell cycle changes are analyzed using cells expressing a fluorescent ubiquitination-based cell cycle indicator (Fucci). Cell cycle checkpoint activation is the immediate response of cells exposed to radiation. Indeed, cell cycle arrest was observed only in NIS-expressing cells capable of uptake [^{131}I]NaI. Consistent with the absorbed dose simulation results, cell cycle arrest was observed in all regions of the 3D tumor spheroid. This result is also estimated because the tissue penetration range of β-rays emitted from ^{131}I is about 2 mm, which is longer than the diameter of the 3D tumor spheroid.

The limitations of this study are as follows. First, the reliability of the parameters used in the MIRDcell simulation could not be verified. The measurement error may have been amplified

because the measured γ-counter had a measurement limit of 1 Bq and was calibrated with ^{131}I at a shallow dose of 3.7 kBq. Second, it was insufficient to ensure that the simulation data were biologically correct. Cell cycle analysis using Fucci can only know the absorbed dose range, and the therapeutic effect can be confirmed only when cell death is confirmed.

Third, the MIRDcell program has limitations in implementing the actual *in vitro* environment. Cells are not perfectly spherical and vary in size and character. Radionuclides have uncontrollable biological parameters, such as differential expression of target proteins, different radioresistance, and a hypoxic environment.

In conclusion, this study demonstrated the potential of 3D tumor spheroids as a preclinical tumor model for basic research into radiopharmaceuticals. MIRDcell has been evaluated as a tool for microdosimetry and prediction of cell survival response. Applying MIRDcell simulation of 3D tumor spheroids to radiopharmaceutical research requires understanding preclinical and clinical differences. The distribution of radiopharmaceuticals in tissues, the residence time of radiopharmaceuticals within cells, and the cellular uptake of radiopharmaceuticals differ between preclinical and clinical studies. Estimating these

biological parameters solely through computations may be inappropriate. Because biological parameters significantly impact microdosimetry, parameter determination experiments should precede dosimetry simulations.

REFERENCES

1. Baskar R, Lee KA, Yeo R, Yeoh KW. Cancer and radiation therapy: current advances and future directions. Int J Med Sci. 2012;9(3):193-9.

2. Katugampola S, Wang J, Rosen A, Howell RW. MIRD Pamphlet No. 27: MIRDcell V3, a Revised Software Tool for Multicellular Dosimetry and Bioeffect Modeling. J Nucl Med. 2022;63(9):1441-9.

3. Sofou S. Radionuclide carriers for targeting of cancer. Int J Nanomedicine. 2008;3(2):181-99.

4. Sgouros G, Bodei L, McDevitt MR, Nedrow JR. Radiopharmaceutical therapy in cancer: clinical advances and challenges. Nat Rev Drug Discov. 2020;19(9):589-608.

5. Katt ME, Placone AL, Wong AD, Xu ZS, Searson PC. In Vitro Tumor Models: Advantages, Disadvantages, Variables, and Selecting the Right Platform. Front Bioeng Biotechnol. 2016;4:12.

6. Kapałczyńska M, Kolenda T, Przybyła W, Zajączkowska M, Teresiak A, Filas V, et al. 2D and 3D cell cultures – a comparison of different types of cancer cell cultures. Arch Med Sci. 2018;14(4):910–9.

7. de Kruijff RM, van der Meer A, Windmeijer CAA, Kouwenberg JJM, Morgenstern A, Bruchertseifer F, et al. The therapeutic potential of polymersomes loaded with ^{225}Ac evaluated in 2D and 3D in vitro glioma models. Eur J Pharm Biopharm. 2018;127:85–91.

8. Onozato Y, Kaida A, Harada H, Miura M. Radiosensitivity of quiescent and proliferating cells grown as multicellular tumor spheroids. Cancer science. 2017;108(4):704–12.

9. Katugampola S, Wang J, Prasad A, Sofou S, Howell RW. Predicting response of micrometastases with MIRDcell V3: proof of principle with ^{225}Ac–DOTA encapsulating liposomes that produce different activity distributions in tumor spheroids. Eur J Nucl Med Mol Imaging. 2022;49(12):3989–99.

10. Doctor A, Seifert V, Ullrich M, Hauser S, Pietzsch J. Three–Dimensional Cell Culture Systems in Radiopharmaceutical Cancer

Research. Cancers (Basel). 2020;12(10):2765.

11. Loevinger R, Berman M. MIRD. Pamphlet no. 1. J Nucl Med. 1968:7.

12. Weber DA. The MIRD method of estimating absorbed dose. Brookhaven National Lab., 1991.

13. Vaziri B, Wu H, Dhawan AP, Du P, Howell RW. MIRD pamphlet no. 25: MIRDcell V2. 0 software tool for dosimetric analysis of biologic response of multicellular populations. Journal of Nuclear Medicine. 2014;55(9):1557-64.

14. Kim YH, Youn H, Na J, Hong KJ, Kang KW, Lee DS, et al. Codon-optimized human sodium iodide symporter (opt-hNIS) as a sensitive reporter and efficient therapeutic gene. Theranostics. 2015;5(1):86-96

15. O'donoghue J, Zanzonico P, Humm J, Kesner A. Dosimetry in Radiopharmaceutical Therapy. Journal of Nuclear Medicine. 2022;63(10):1467-74.

16. O'donoghue J, Bardies M, Wheldon T. Relationships between tumor size and curability for uniformly targeted therapy with beta-emitting radionuclides. Journal of Nuclear Medicine. 1995;36(10):1902-9.

17. Howell RW, Rao DV, Sastry KS. Macroscopic dosimetry for radioimmunotherapy: nonuniform activity distributions in solid tumors. Med Phys. 1989;16(1):66-74.

18. Solanki JH, Tritt T, Pasternack JB, Kim JJ, Leung CN, Domogauer JD, et al. Cellular response to exponentially increasing and decreasing dose rates: implications for treatment planning in targeted radionuclide therapy. Radiation research. 2017;188(2):221-34.

19. Leung CN, Canter BS, Rajon D, Bäck TA, Fritton JC, Azzam EI, et al. Dose-dependent growth delay of breast cancer xenografts in the bone marrow of mice treated with ^{223}Ra: the role of bystander effects and their potential for therapy. Journal of Nuclear Medicine. 2020;61(1):89-95.

20. Canter BS, Leung CN, Fritton JC, Bäck T, Rajon D, Azzam EI, et al. Radium-223-Induced Bystander Effects Cause DNA Damage and Apoptosis in Disseminated Tumor Cells in Bone MarrowRadium-223-Induced Bystander Effects. Molecular Cancer Research. 2021;19(10):1739-50.

21. Neti PV, Howell RW. Isolating effects of microscopic nonuniform distributions of ^{131}I on labeled and unlabeled cells. Journal of Nuclear Medicine. 2004;45(6):1050-8.

22. Rajon D, Bolch WE, Howell RW. Lognormal distribution of cellular uptake of radioactivity: Monte Carlo simulation of irradiation and cell killing in 3-dimensional populations in carbon scaffolds. Journal of Nuclear Medicine. 2011;52(6):926-33.

23. Neti PV, Howell RW. Log normal distribution of cellular uptake of radioactivity: implications for biologic responses to radiopharmaceuticals. Journal of Nuclear Medicine. 2006;47(6):1049-58.

24. Sakaue-Sawano A, Kurokawa H, Morimura T, Hanyu A, Hama H, Osawa H, et al. Visualizing spatiotemporal dynamics of multicellular

cell-cycle progression. Cell. 2008;132(3):487-98.

25. Sakaue-Sawano A, Yo M, Komatsu N, Hiratsuka T, Kogure T, Hoshida T, et al. Genetically encoded tools for optical dissection of the mammalian cell cycle. Molecular cell. 2017;68(3):626-40. e5.

26. Shimono H, Kaida A, Homma H, Nojima H, Onozato Y, Harada H, et al. Fluctuation in radioresponse of HeLa cells during the cell cycle evaluated based on micronucleus frequency. Scientific Reports. 2020;10(1):1-9.

27. Yu KH, Youn H, Song MG, Lee DS, Chung JK. The Effect of Tanespimycin (17-AAG) on Radioiodine Accumulation in Sodium-Iodide Symporter Expressing Cells. Nucl Med Mol Imaging. 2012;46(4):239-46.

28. James MB, Giorgio TD. Nuclear-associated plasmid, but not cell-associated plasmid, is correlated with transgene expression in cultured mammalian cells. Molecular Therapy. 2000;1(4):339-46.

29. Portulano C, Paroder-Belenitsky M, Carrasco N. The Na+/I-symporter (NIS): mechanism and medical impact. Endocrine reviews. 2014;35(1):106-49.

30. Ravera S, Reyna-Neyra A, Ferrandino G, Amzel LM, Carrasco N. The sodium/iodide symporter (NIS): molecular physiology and preclinical and clinical applications. Annual review of physiology. 2017;79:261.

31. Spitzweg C, Morris JC. The sodium iodide symporter: its pathophysiological and therapeutic implications. Clinical endocrinology. 2002;57(5):559-74.

32. Chung JK. Sodium iodide symporter: its role in nuclear medicine. Journal of Nuclear Medicine. 2002;43(9):1188-200.

33. Paroder-Belenitsky M, Maestas MJ, Dohán O, Nicola JP, Reyna-Neyra A, Follenzi A, et al. Mechanism of anion selectivity and stoichiometry of the Na+/I-symporter (NIS). Proceedings of the National Academy of Sciences. 2011;108(44):17933-8.

34. Pawlik TM, Keyomarsi K. Role of cell cycle in mediating sensitivity to radiotherapy. International Journal of Radiation Oncology* Biology* Physics. 2004;59(4):928-42.

35. Syljuåsen RG. Cell Cycle Effects in Radiation Oncology. In: Wenz F, editor. Radiation Oncology. Cham: Springer International Publishing; 2019. 1-8.

36. Tamborino G, Saint-Hubert D, Struelens L, Seoane DC, Ruigrok EA, Aerts A, et al. Cellular dosimetry of [^{177}Lu]Lu-DOTA-[Tyr3] octreotate radionuclide therapy: the impact of modeling assumptions on the correlation with in vitro cytotoxicity. EJNMMI physics. 2020;7(1):1-19.

37. Petrich T, Helmeke H-J, Meyer G, Knapp W, Pötter E. Establishment of radioactive astatine and iodine uptake in cancer cell lines expressing the human sodium/iodide symporter. European journal of nuclear medicine and molecular imaging. 2002;29(7):842-54.

38. Read ML, Brookes K, Thornton CE, Fletcher A, Nieto HR, Alshahrani M, et al. Targeting non-canonical pathways as a

strategy to modulate the sodium iodide symporter. Cell chemical biology. 2022;29(3):502-16.

39. Mohammadi S, Loushab ME, Toossi MTB. Geant4 Modeling of Cellular Dosimetry of ^{188}Re: Comparison between Geant4 Predicted Surviving Fraction and Experimentally Surviving Fraction Determined by MTT Assay. Journal of Biomedical Physics & Engineering. 2021;11(4):473.

40. Chan HS, De Blois E, Morgenstern A, Bruchertseifer F, De Jong M, Breeman W, et al. In Vitro comparison of ^{213}Bi-and ^{177}Lu-radiation for peptide receptor radionuclide therapy. PLoS One. 2017;12(7):e0181473.

41. Reijonen V, Kanninen LK, Hippeläinen E, Lou Y-R, Salli E, Sofiev A, et al. Multicellular dosimetric chain for molecular radiotherapy exemplified with dose simulations on 3D cell spheroids. Physica Medica. 2017;40:72-8.

42. Yu L-S, Jhunjhunwala M, Hong S-Y, Yu L-Y, Lin W-R, Chen C-S. Tissue Architecture Influences the Biological Effectiveness of Boron Neutron Capture Therapy in In Vitro/In Silico Three-

Dimensional Self-Assembly Cell Models of Pancreatic Cancers. Cancers. 2021;13(16):4058.

43. Zhao L, Kroenke C, Song J, Piwnica-Worms D, Ackerman J, Neil J. Intracellular water-specific MR of microbead-adherent cells: the HeLa cell intracellular water exchange lifetime. NMR in Biomedicine. 2008;21(2):159-64.

44. Spitzweg C, Nelson P, Wagner E, Bartenstein P, Weber W, Schwaiger M, et al. The sodium iodide symporter (NIS): novel applications for radionuclide imaging and treatment. Endocrine-related cancer. 2021;28(10):T193-T213.

45. Kumar C, Jayakumar S, N Pandey B, Samuel G, Venkatesh M. Cellular and molecular effects of beta radiation from I-131 on human tumor cells a comparison with gamma radiation. Current Radiopharmaceuticals. 2014;7(2):138-43.

46. Petrich T, Quintanilla-Martinez L, Korkmaz Z, Samson E, Helmeke HJr, Meyer GJr, et al. Effective cancer therapy with the alpha-particle emitter [^{211}At] astatine in a mouse model of genetically modified sodium/iodide symporter-expressing tumors. Clinical

cancer research: an official journal of the American Association for Cancer Research. 2006;12(4):1342-8.

47. Deycmar S, Faccin E, Kazimova T, Knobel PA, Telarovic I, Tschanz F, et al. The relative biological effectiveness of proton irradiation in dependence of DNA damage repair. The British Journal of Radiology. 2020;93(1107):20190494.

48. Van Sande J, Massart C, Beauwens R, Schoutens A, Costagliola S, Dumont JE, et al. Anion selectivity by the sodium iodide symporter. Endocrinology. 2003;144(1):247-52.

49. Pouget JP, Constanzo J. Revisiting the radiobiology of targeted alpha therapy. Frontiers in Medicine. 2021:1125.

50. Shen D, Marsee D, Schaap J, Yang W, Cho J, Hinkle G, et al. Effects of dose, intervention time, and radionuclide on sodium iodide symporter (NIS)-targeted radionuclide therapy. Gene therapy. 2004;11(2):161-9.

51. Watabe T, Kaneda-Nakashima K, Liu Y, Shirakami Y, Ooe K, Toyoshima A, et al. Enhancement of ^{211}At uptake via the sodium iodide symporter by the addition of ascorbic acid in targeted α-therapy of thyroid cancer. Journal of Nuclear Medicine. 2019;60(9):1301-7.

52. Jia S, Ge S, Fan X, Leong KW, Ruan J. Promoting reactive oxygen species generation: a key strategy in nanosensitizer-mediated radiotherapy. Nanomedicine. 2021;16(9):759-78.

53. Carlin S, Mairs RJ, Welsh P, Zalutsky MR. Sodium-iodide symporter (NIS)-mediated accumulation of [^{211}At] astatide in NIS-transfected human cancer cells. Nuclear medicine and biology. 2002;29(7):729-39.

국문 초록

서론: 방사성의약품을 이용한 항암 치료 시, 방사성의약품에 대한 세포반응과 치료효과를 예측하기 위해서는 종양이 흡수하는 방사선량을 알아야 한다. 그러나 방사선의 흡수량을 실제로 계산하기 위한 연구는 아직 미흡하다. 3 차원 종양 스페로이드에 위치한 방사성의약품의 분포 정도를 측정하고, 다양한 매개변수에 의한 방사선 흡수량의 변화를 계산함으로써, 방사성 의약품의 치료효과 예측에 도움을 줄 수 있다.

방법: 치료용 방사성요오드 ^{131}I 을 세포 안으로 전달하기 위해, 나트륨요오드수송체(NIS)를 세포에 발현시켰다. NIS 발현 세포를 이용하여 3 차원 종양 스페로이드를 제작하고 ^{131}I 을 흡수시켰다. 3 차원 종양 스페로이드를 해리하여 ^{131}I 분포를 측정하였다. MIRDcell 을 이용하여 3 차원 종양 스페로이드의 방사선 흡수 선량 및 세포 생존 반응을 계산하였다. 3 차원 종양 스페로이드의 세포에서 발현되는 형광 유비퀴틴화 기반 세포 주기 표시기(Fucci)를 영상화하여 세포 주기를 분석하였다.

결과: [^{131}I]NaI 방사능에 대한 3 차원 종양 스페로이드의 중심 거리를 대수정규분포 곡선에 맞추었다. 시뮬레이션 결과, 3 차원

종양 스페로이드 정중앙 부분의 흡수선량은 방사능 분포에 따라 5 배 이상의 차이가 존재하였다. 세포 내 최대 평균 방사능이 일정할 때, 비교적 낮은 이온화 에너지와 높은 투과 범위를 가진 ^{131}I 은, 비교적 높은 이온화 에너지와 낮은 투과범위를 가진 ^{211}At 보다 더 많은 세포를 손상시켰다. 방사능의 체류 시간(residence time)에 MIRD 공식의 'time−integrated activity coefficient(1.44 × ^{131}I 의 물리적 반감기)' 를 대입하면 세포 생존율이 0.1% 미만으로 예측되지만, 방사능의 체류 시간에 '세포 내 요오드 체류 시간(1.44×세포 내 ^{131}I 의 반감기)'을 대입하면 세포 생존율이 10% 이상으로 예측되었다. 전체 세포 생존율은 ^{131}I 로 표지 된 세포의 수가 증가할수록 감소하였지만, ^{131}I 로 표지 된 세포 생존율과 ^{131}I 로 표지 되지 않은 세포 생존율 간 유의한 차이는 없었다.

^{131}I 은 3 차원 종양 스페로이드의 외부에 주로 분포하지만, ^{131}I 에서 방출되는 방사선은 3 차원 종양 스페로이드의 모든 영역에서 흡수되었다. 세포주기 분석 결과 또한, 3 차원 종양 스페로이드의 모든 영역에서 세포주기 정지가 관찰되었다.

결론: 이 연구는 방사성 의약품에 대한 기본 연구를 위한 전임상 종양 모델로서 3D 종양 스페로이드의 가능성을 입증하였다. MIRDcell 은 미세 선량 측정 및 세포 생존 반응 계산을 위한

도구로서 평가되었다. 3D 종양 스페로이드의 MIRDcell 시뮬레이션을 방사성 의약품 연구에 적용하기 위해서는, 전임상과 임상의 차이를 이해해야 한다. 조직 내 방사성 의약품의 분포, 세포 내 방사성 의약품의 체류 시간, 방사성 의약품의 세포 흡수율은 전임상 연구와 임상 연구 간 차이가 존재한다. 계산으로만 이러한 생물학적 매개변수를 추정하는 것은 부적절할 수 있다. 미세 선량분석에 생물학적 매개변수가 큰 영향을 미치기 때문에, 미세 선량분석 시뮬레이션 이전에 매개변수를 결정하기 위한 전임상 실험이 선행되어야 한다.

주요어 : 미세 선량분석 시뮬레이션, 3차원 종양 스페로이드, MIRDcell, 방사성 요오드: ^{131}I, 방사능, 방사선 흡수량, 방사능 분포, 세포생존 반응, 형광 유비퀴틴화 기반 세포 주기 표시기(Fucci)
학 번 : 2020-28141